University of Southern Queensland

Faculty of Health, Engineering and Sciences

Stability analysis on a fossil fuel ash dam using a 3D numerical method

A dissertation submitted by

Mr. Vernon Marc Erasmus

Bachelor of Science (Honours) Construction Management

In fulfilment of the requirements of

ENG4111 and 4112 Research Project

towards the degree of

Bachelor of Engineering (Honours) Civil Engineering

Submitted October 2020

Abstract

South Africa will be producing power using Fossil fuel power stations for the foreseeable future. Large volumes of ash are produced during this process, which is disposed using wet or dry systems. Optimizing these dumps will reduce the power station's environmental impact and costs due to the reduction of land area required and additional lining and infrastructure costs.

As the processing power of computers increase, more complex numerical and mathematical simulations are possible. This study will use numerical modelling software, FLAC3D, to assess the slope stability of an ash dam. This model is then compared with the more conventional and sufficient Morgenstern-Price method using Slope/W. Some of the major disadvantages of most conventional 2D models is that the effect of irregular shapes is not taken into consideration and that selecting of a most vulnerable section is subjective. 2D models are also more conservative than 3D models.

During this study a factor of safety of 1.5 is maintained as a stable slope and the effect of earthquakes is not evaluated due to South Africa's location in respect to fault lines.

Keywords: Slope stability, ash dam, ash dump, ash impoundment, ash pond, FLAC3D, fossil fuel power station, coal fire power station

University of Southern Queensland

Faculty of Health, Engineering and Sciences

ENG4111 & ENG4112 Research Project

Limitations of Use

Certification

I certify that the ideas, designs and experimental work, results, analyses and conclusions set out in this dissertation are entirely my own effort, except where otherwise indicated and acknowledged.

I further certify that the work is original and has not been previously submitted for assessment in any other course or institution, except where specifically stated.

Vernon Marc Erasmus

Student Number: [redacted]

Contents

Table of figures

Table of tables

Definitions

Rate of rise - The rate at which the dam is heightened given in raise per year. This limits the size of lifts.

Failure - A stability failure unless directly mentioned to the contrary. Excluding failures like seeping through the dam wall.

Phreatic surface - Also called the water table, this is the height at which the pore water pressure is zero (atmospheric) when the pore water pressure is measured relative to atmospheric pressure (Craig, 2004).

Abbreviations

ANCOLD	-	Australian National Committee on Large Dams
DCP	-	Dynamic Cone Penetration
FOS	-	Factor of Safety
LL	-	Liquid Limit
m.a.m.s.l	-	meters above mean sea level
ML	-	Inorganic silt with very fine Orange-brown material
GM	-	Grading modulus
PI	-	Plasticity index
PE	-	Potential expansiveness
SRM	-	Strength Reduction Method
NP	-	Non-plastic
LS	-	Linear shrinkage
MDD	-	Maximum dry density
USC	-	Unified soil classification
OMC	-	Optimum moisture content

1 Introduction

Arnot Power Station, South Africa, is a coal fire power station and uses a wet ashing system. This system transports ash to an ash dam where the ash settles. The water is then re-used to transport more ash. The walls are constructed using fly-ash and the coarse ash is poured into the middle.

This research looks at the slope stability of Arnot's ash dam, which is reaching the end of its life. This will be done by providing a slope analysis using FLAC3D and Slope/W.

Currently there is no standard for dealing with ash dams in South Africa, and the standard for tailing dams is used. Tailing dams are similar in most respects, but for dealing with mine discard.

The literature review looks at the different limit equilibrium methods, namely the Ordinary-, Bishop's simplified-, Method of slices for steady state seepage, Spencer's solution, Morgenstern's-, Morgenstern and Price- and Fellenius or Swedish- method.

Numerical methods are also looked at. The continuum methods looked at includes; finite differencing method (FDM), finite element method (FEM), boundary element method (BEM) and finite volume method (FVM). The discontinuum methods discussed are; the distinct element method (DEM), discontinuous deformation analysis (DDM) and the bonded particle method (BPM).

The Morgenstern-Price method is applied using Slope/W and the FVM is applied using FLAC3D and setting up a model using SketchUp Pro.

A brief sensitivity analysis is done in FLAC3D where the effects of changing the cohesion, friction angle, Young's modulus and Poisson's ratio is assessed.

1.1 Background

Arnot power station is reaching the end of its life. The station has built two additional ash dams during its life, which forms one dam complex with the original dam. The aim is to start and operate the complex as one dam near the end of its life. This provides an opportunity to assess a dam's stability close to the end of its life.

1.1.1 Ash production at power stations

Coal fired power stations create large amounts of ash, as waste (Ayob et al., 2014). The ash can be divided into two distinctly different types, namely coarse ash and fly-ash. Coarse ash is also referred to as bottom ash (Zielke-Olivier & Vermeulen, 2019).

There are two major systems of conveying this ash used in South Africa, one being a wet system and the other a dry system. The dry system comprises of conveyor systems depositing the ash onto dumps or landfill sites. Using landfill sites is the normal method (Ayob et al., 2014). In South Africa the older system is the wet system. Where the wet system is used, the ash is made into a slurry, which is deposited onto ash dams. The fly-ash is used to build the dam's walls, and coarse ash is filled into the dam's centre. This research will be centred around this wet system.

During the combustion of coal in the boiler of a power station approximately 10% of the ash will fall into the boiler's bottom hopper filled with water. This ash is coarse and will be sent through crushers before entering a sump, from which slurry pumps take suction. The slurry pumps then deposit the ash on a ash dam. Coarse ash has a grain size comparable to that of sand.

The remaining 90% will be sucked out of the boiler by large fans. This draft created will first pass through an air-heater. Here the heat in the draft will be transferred to heat sinks that will then pass the heat onto a cold draft. This newly heated cold air will be used as supply to the boiler for combustion. The cooled dirty draft then passes through a precipitator or bag filter house, through the fans and out through a smokestack or chimney. In this study, bag filters are used.

The fly-ash that was caught by the bags are then cleaned off pneumatically and falls into hoppers. The hoppers are extracted with hydrovacs that create a water-ash slurry, that is sent to an ash sump. This is the same sump used for coarse ash. The fly ash has a consistency similar to clay and is used to build the dam walls as shown in figure 1. Because fly-ash is used for the dam walls and coarse ash as infill, the cleaning of the coarse ash hoppers and fly-ash hoppers are not done simultaneously. Coarse ash is removed during the night and fly ash during the day. This enables, through the use of pipework and valves, that the coarse- and fly-ash can be deposited as required. Removing fly-ash during the day also allows more accurate building of walls because of improved visibility during the light of day.

Figure 1 Day wall and pool area (Google, 2020)

Each time ash is deposited on a wall, sufficient settling time must be given to allow dewatering and sedimentation (Knutsson, 2015). At Arnot this is approximately 12 days.

1.1.2 Arnot Power Station's Ash Dam

Construction of Arnot power station started in 1968 (Eskom, 2019). It has one ash dam complex that was built in three stages. They are individually called Ash dam 1, Ash dam 2 and Flamingo pan and is shown in figure 2.

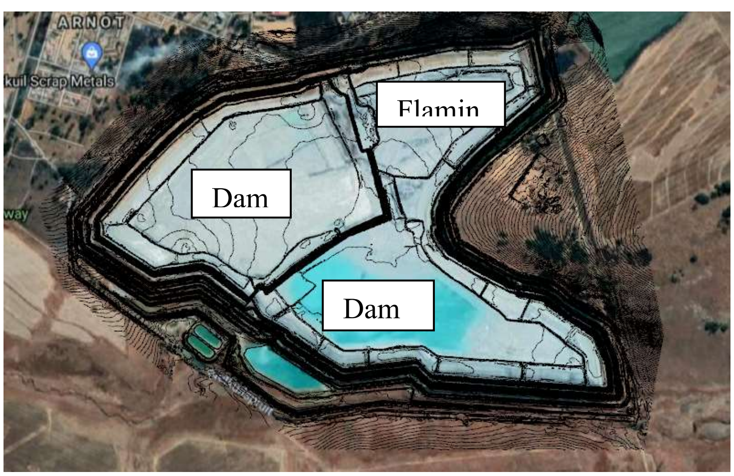

Figure 2 Google Maps Aerial View with Dam Names and Aerial Survey Overlay

Ash dam 2 and Flamingo pan has no toe-drains. Toe-drains have the function to relate the seepage water through the dam wall, without daylighting in an uncontrolled manner, which could lead to erosion. This seepage water will also have an negative effect on the overall stability of the dam and increase the risk of a slip (Verdeș, 2017).

Ash dam 1 was first constructed in the 1960s, and as the need for ashing-capacity grew, an additional dam was constructed to the south called Ash dam 2. Ash dam 2 was built on top of the stream, which means that the stream had to be diverted, refer to figure 4. This river left behind a very soft Grey-black clay, which now forms part of the foundation material. A third dam was created by filling up Flamingo Pan, which used to be a natural water body fed from a spring, with ash and the created ash dam to the north east was then also named so. The water that ran out of water body into the stream was rerouted through a soil channel on the western side of the dam, refer to figure 3.

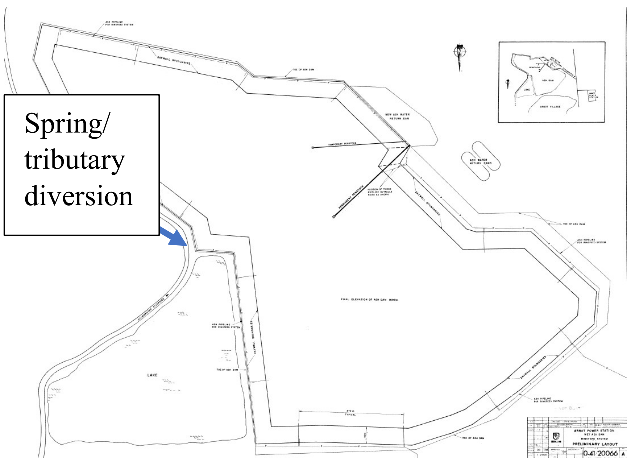

Figure 3 Flamingo pan shown as "Lake"

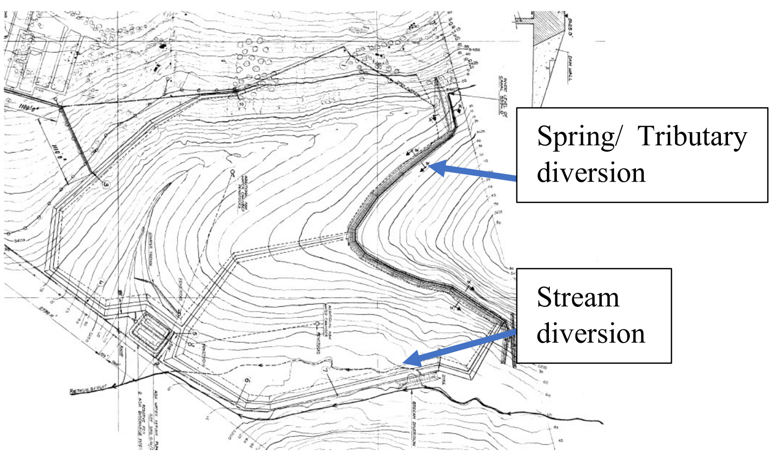

Figure 4 River running through the ash dam

1.1.2.1 Tributary/ spring water diversion

The diversion channel runs the eastern length of the ash impoundment as shown in figure 3 and 4, and the original design is given in figure 5. The channel is close to the toe of the dam.

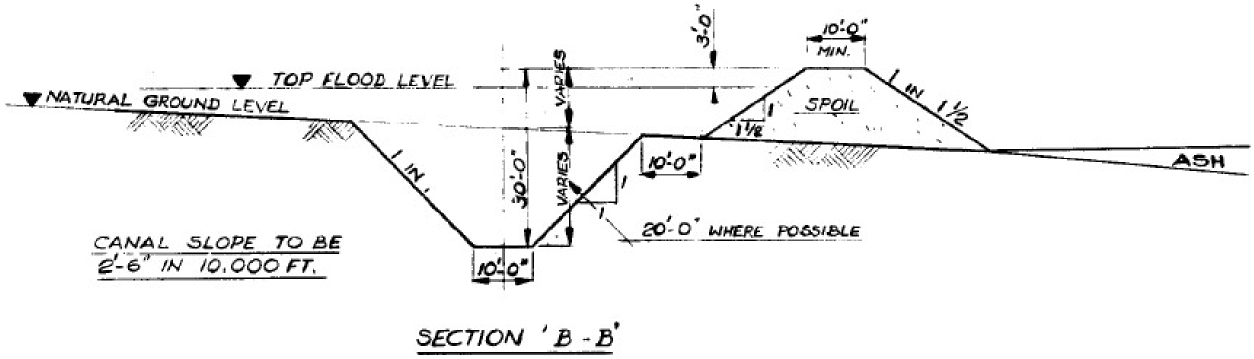

Figure 5 Original design of spring diversion

As can be seen from figure 5, the slopes of this channel are 45° steep and several slips can be seen in the channel, please refer to figure 6. What can also be seen in figure 6 is how densely the channel has been overgrown with trees. It is assumed that these trees act as soil anchors and stabilizes the slope.

Figure 6 Localised slip as viewed from above

1.1.2.2 Area where Ash dam 2 and Flamingo Pan meets

An irregular shape is created where Ash dam 2 and Flamingo pan meets. This is shown in figure 7.

Figure 7 Irregular shape created where Ash dam 2 and Flamingo pan meets (Google, 2020)

This shape creates three-dimensional flow which dramatically increases the phreatic surface. The area is quite wet, and water is seen daylighting at the toe where the two shapes meet.

1.1.2.3 Phreatic surface

The phreatic surface is monitored using piezometers located around the ash dam. Each location consists of three piezometers to represent the cross section of the dam, as shown in figure 8. The levels are assessed monthly against safe operating levels.

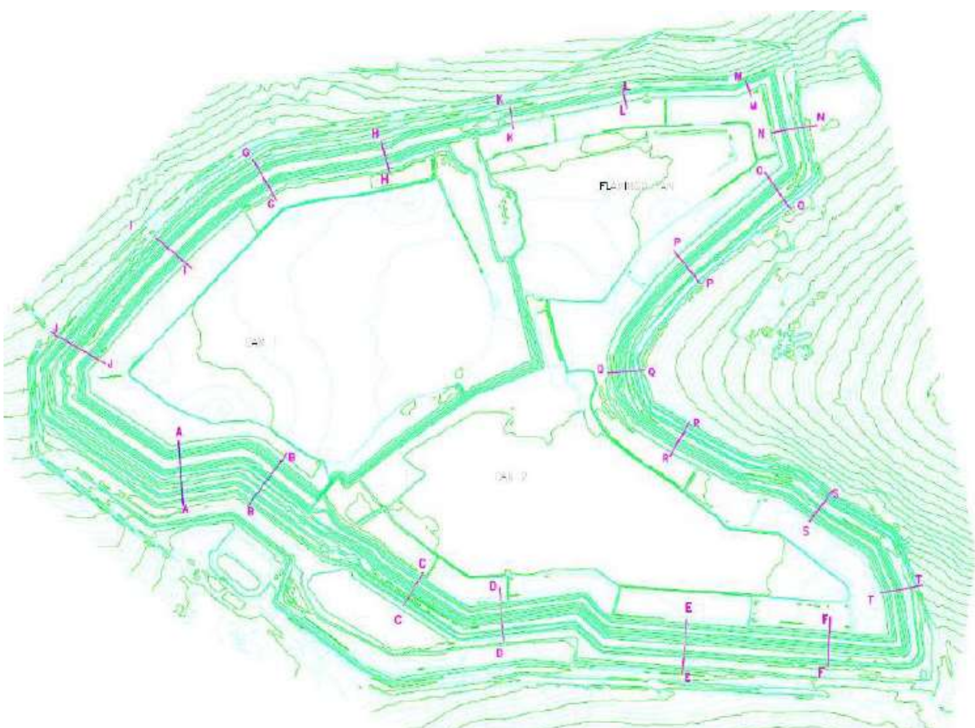

Figure 8 Location of Piezometers (Barnard, 2010)

1.1.2.4 Toe-drains

The geotechnical property that has the largest effect on the rate of seepage is the coefficient of permeability, or hydraulic conductivity (*k*) (Craig, 2004; Das & Sobhan, 2018). Other factors include the hydraulic gradient (*i*) and the cross area (*A*) to form Darcy's empirical law (Craig, 2004; Das & Sobhan, 2018):

q = Aki or velocity (v) = q/A = ki

Where toe-drains are present, the phreatic surface follow the form of a basic parabola as shown in figure 9 (Craig, 2004):

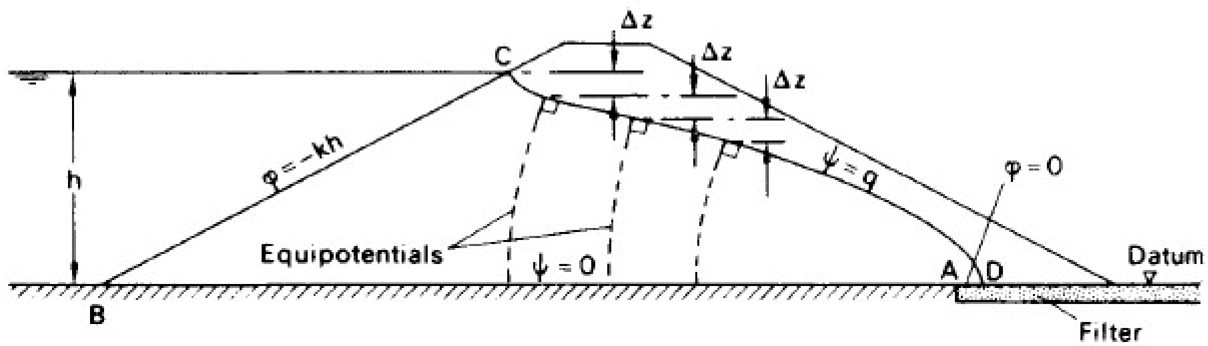

Figure 9 Seepage through a homogeneous embankment with a toe-drain (Craig, 2004)

Where no toe-drains are present and an impervious base is present the following phreatic surface is presented as shown in figure 10 (Das & Sobhan, 2018):

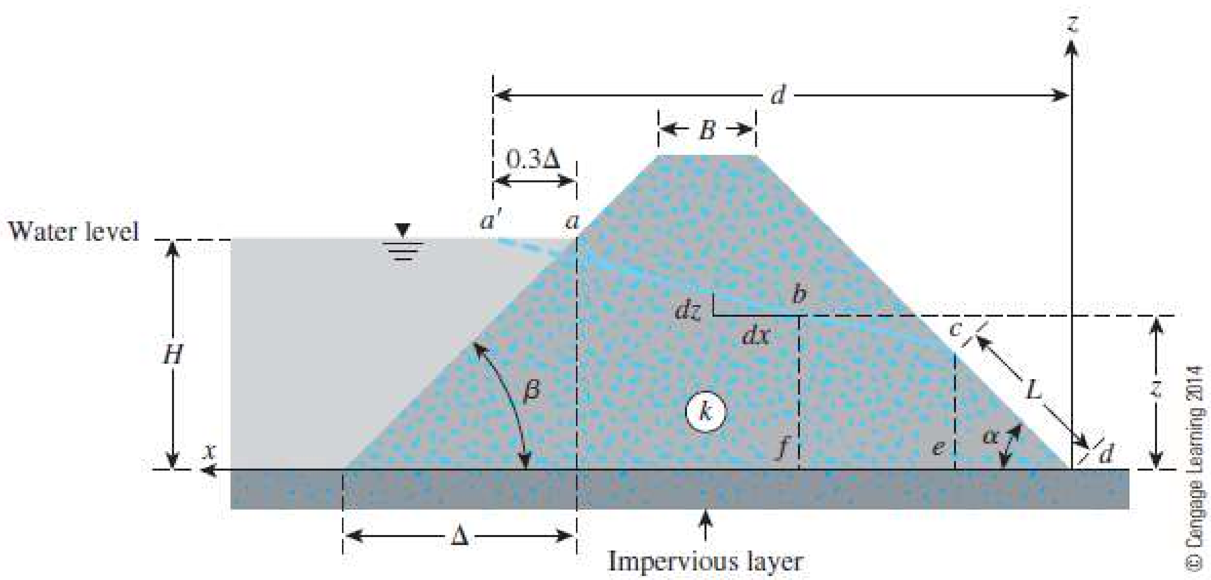

Figure 10 Flow through an earth dam constructed over an impervious base (Das & Sobhan, 2018)

Because no toe drains are present and because of the low slope angle of the wall (1:3), the phreatic surface is very close to the surface of the wall.

1.1.3 Ash qualities

The fly-ash to coarse ash ratio produced from coal fired power stations is normally 80% to 20% (Ayob et al., 2014). The specific gravity of fly ash is 2.22, and for coarse ash is 2.54 (Ayob et al., 2014).

The density of fly-ash can range dramatically from 1.01g/cm³ to 1.78g/cm³ (Arpita et al., 2019). This is largely ascribed to compaction.

The shear strength of fly-ash increases dramatically, from 7 days of curing to 28 days, from 36.66kPa to 309.23kPa (Ayob et al., 2014). This is attributed to pozzolanic reaction, agglomerates bonded particles due to crystal growth (Calcite, Quartz and Moissanite), and the hydrolysis process (cementing) (Ayob et al., 2014). Fly ash has a higher pH compared to bottom ash showing higher free lime and alkaline oxides (Ayob et al., 2014).

This ash contain several elements that are hazardous to ones health like mercury, chromium, lead, antimony, cadmium and arsenic (Ayob et al., 2014). This ash pollutes the environment (Ayanda, Fatoki, Adekola, & Ximba, 2012; Ayob et al., 2014).

1.1.4 Why use the standard for tailings dams on ash dams?

There is currently no specific standard of practice for the construction of Ash dams, thus the standard for tailing dams is used which is named SABS:0286 "Mine residue". Tailings dams are very similar to ash dams, in that it is also used to dispose of waste with geotechnical properties. In both cases waste can be pumped in the form of a slurry to impounds called either tailing dams, in the case of mine residue, or ash dams or impoundments for power utilities (Knutsson, 2015). Tailings is the name for waste from mining activities from which the valuable minerals have been recovered (Knutsson, 2015; Ozcan, Ulusay, & Isik, 2013). Each tailing dam is different because of the different material it composes off (Knutsson, 2015). Thus, tailings material has its origin from mining activities, which could be coal-, gold-, zinc-, rear minerals-, copper-mining or any other mining activity (Knutsson, 2015). Also, the geological conditions and construction methods will vary from mine to mine (Knutsson, 2015).

In South Africa, tailing dams need to be designed for overall stability, local instability, surface erosion, and deformation for high hazard residue deposits (SABS:0286, 1998). Special care needs to be taken for pore water pressure, which will limit the rate of rise (SABS:0286, 1998). Also, where flow nets are drawn, one must account for anisotropy, the water on top of the dump, and geotechnical differences through foundation and building material (SABS:0286, 1998). Where homogeneous and isotropic material is present, circular slip surfaces may be used, otherwise non-circular failure surfaces will be required (SABS:0286, 1998).

1.1.5 Risk of ash dam failures

Frequently tailing dams fail around the world (Knutsson, 2015). Failure of ash dams can lead to loss of life, irreversible environmental damage and financial losses (Ozcan et al., 2013).

There was approximately 8 tailing dam failures per decade in the 1940s and 1950s, 50 during the 60s, 70s and 80s and approximately 20 during the 90s and 2000s (Knight, 2015). The failure modes of tailing dams is overtopping, foundation failure, piping, slope instability, liquefaction and erosion (Ozcan et al., 2013). The amount of failure with associated causes are given in figure 11 and 12 below and they are categorised per continent in figure 13.

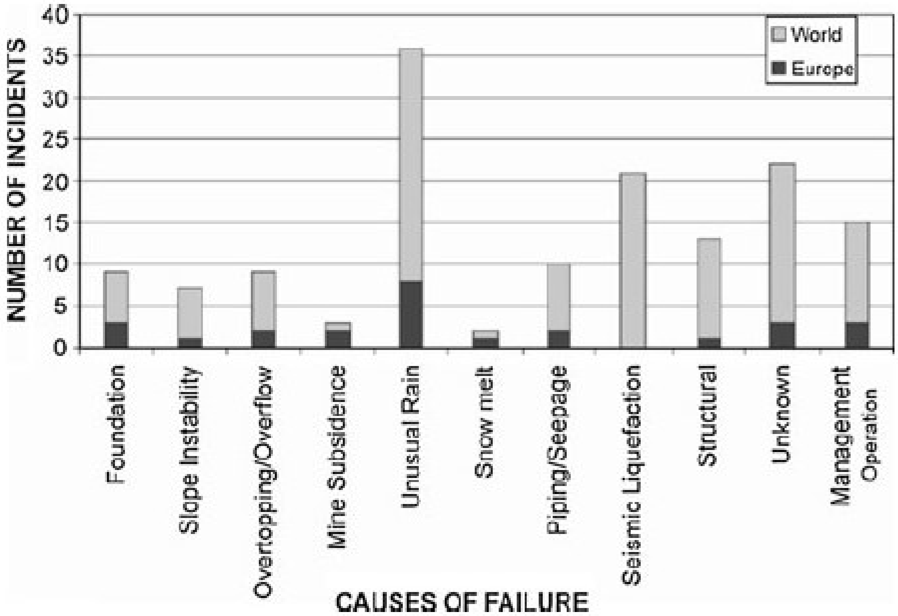

Figure 11 Causes of failures (Ozcan et al., 2013)

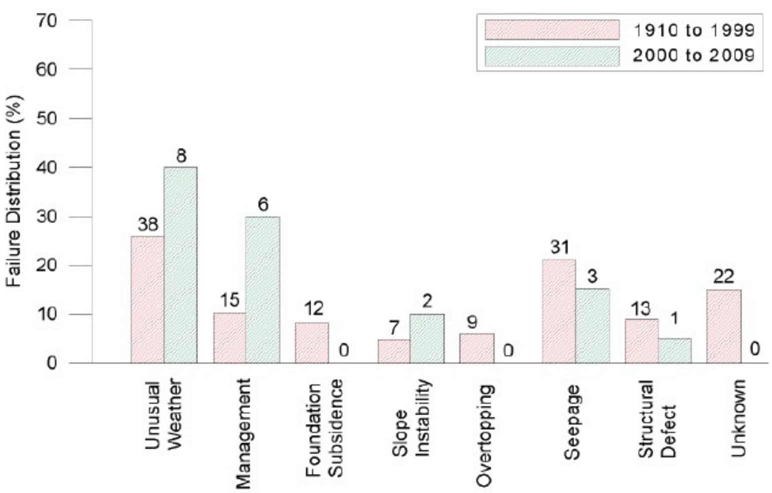

Figure 12 Causes of failure (Knight, 2015)

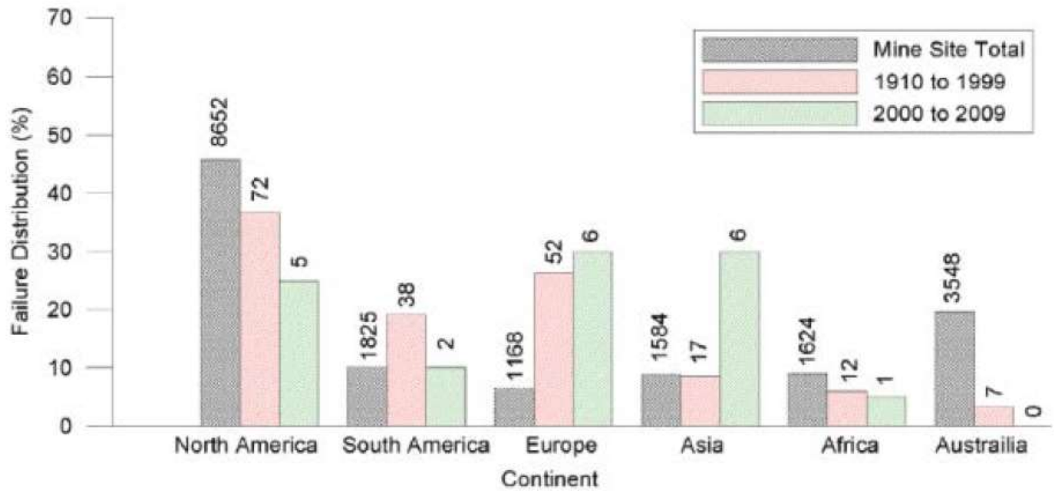

Figure 13 Tailing dam failure per continent (Knight, 2015)

1.2 Problem statement

Several years have gone by since the last stability analysis of Arnot's Ash Dam. In this time the dam has grown substantially in height. Access to computers and their processing power have increased dramatically in that time. To enable effective management of a dam, one must know the factor of safety of the facility. Thus, a need now exists to assess the stability of the ash dam using the current profiles, which will be done by using the geotechnical properties of the ash and surrounding soils.

The information gathered will be used to assess the dam using the finite volume method through FLAC3D.

1.3 Project Aim

To determine the stability of Arnot Power Station's ash dam using numerical modelling software.

1.4 Objectives of the research

- Provide a decision base for the need of future developments.
- Provide surety of the safety of the ash dam complex.
- Ensure compliance to governing standards.

1.4.1 Motivation

Arnot Power Station's ash dam is reaching the end of its life. An opportunity exists to optimize the dam's construction, or operations to ensure the dam reaches the end of station's life. This research will assist in this by providing the dam's factor of safety, which will provide a starting point for further work.

1.4.2 Significance

This research gives the opportunity to study an ash dam close to the end of its life. A river exists at the toe of the dam in which failures are already seen.

1.5 Research question

Whilst considering the geotechnical properties and geometric properties, what is the stability of the ash dam at Arnot Power Station?

2 Literature review

The literature review will investigate the current practices for stability analysis in tailings- and ash dams. Thereafter, it briefly touches on geotechnical investigations and foundation failure.

2.1 Slope stability analysis

An important part of assessing a dam's stability is determining the factor of safety of the side slopes (Knight, 2015). The failure mechanisms for slopes are the following; fall, topple, slide, spread or flow (Das & Sobhan, 2018). Craig (2004) adds to this by listing; bearing failure below the embankment, internal erosion, surface erosion, hydraulic uplift, and excessive soil deformation causing damage to the surrounding area. When doing a stability analysis these failure mechanisms need to be addressed.

Slope stabilities can be analysed through numerical-, limit equilibrium-, or limit state- methods. Other methods do exist but are seldom used.

2.1.1 Method of slices/ Limit equilibrium method

The limit equilibrium method is also often referred to, as the method of slices and has historically been the more commonly used method (Fredlund & Krahn, 1977; Itasca Consulting Group, 2017b). This is because this method can accommodate a large variety of profiles, water contents and soil types, (Fredlund & Krahn, 1977) but is limited to failures that follow plane, circular, or log spiral patterns (Das & Sobhan, 2018; Itasca Consulting Group, 2017b). Implicit in all these methods it that the stress-strain behaviour of the soil is ductile. In other words the soil does not have a brittle stress-strain curve (Duncan, 1996). It does not accommodate failure mechanisms other than slips because it does not consider stress and strain (Knutsson, 2015). Also, if the shearing resistance drops off after reaching the peak, progressive failure can occur (Duncan, 1996).

When analysing the stability of a slope using the method of slices, one would measure the slopes resistance to sliding, compared to the applied sliding force (Craig, 2004; Das & Sobhan, 2018). When the sliding force is greater than the resisting force, a slip will occur (Craig, 2004; Das & Sobhan, 2018). These slips are normally circular where the soil is monolithic (Craig, 2004; Das & Sobhan, 2018). The resistance to a slide is represented by a factor called the factor of safety (Craig, 2004; Das & Sobhan, 2018). Where the factor of safety is below 1 it would constitute a failure (Craig, 2004; Das & Sobhan, 2018; Knight, 2015). A factor of safety taken above 1.2 would theoretically give a slope that is stable, but there has been dams that have failed at 1.2 (Lin, Zhou, & Li, 2018). This brings into question a factor of safety that is in that region. Ozcan et al. (2013) took 1.2 as acceptable. A factor of safety of 1.5 is more commonly seen as acceptable (Das & Sobhan, 2018; Knutsson, 2015; SABS:0286, 1998). ANCOLD recommends a factor of safety of 1.5 for long-term drained and short-term undrained soils where there is a potential loss of containment, and 1.3 for short-term undrained soils where there is no potential loss of containment (Knight, 2015). A factor of safety of 1.5 is thus deemed the most suitable.

Another issue with the limited equilibrium analysis is the subjective nature of determining the most critical slope which is used for analysis (Shen, Klapperich, Abbas, & Ibrahim, 2012). Most commonly, limited equilibrium analysis and numerical modelling is used to determine the factor of safety on the most critical slopes (Knutsson, 2015).

Of the method of slices: the Ordinary Method of Slices, Morgenstern-Price-, Bishop's simplified-, and Spencer- method, uses interslice forces, and satisfy both force and moment equilibria, which is recommended (Knight, 2015). These have also successfully been adopted into software packages like Slope/W.

Many find that limited equilibrium methods give satisfactory results (Craig, 2004; Das & Sobhan, 2018; Knutsson, 2015). Thus, claims by Knight (2015) that these programs can make designs unsafe by increasing the risk of overlooking geotechnical fundamentals is unfounded.

The method of slices can be done as two-dimensional, which is most commonly done and considers the slope as infinitely wide, or three-dimensionally by converting slices into columns (Das, 2011).

For simple slopes, stability charts can be developed and successfully used (Duncan, 1996).

2.1.1.1 Ordinary Method of Slices

The method of slices is appropriate for layered soil but gives overly conservative results and are thus seldom used (Das & Sobhan, 2018). Pore-water pressure is also not accounted for in this method (Das & Sobhan, 2018; Duncan, 1996). This method is also very inaccurate for flat slopes (Duncan, 1996). It is most appropriate for slopes where the internal angle of friction = 0 and the method does not have numerical problems (Duncan, 1996). A slip circle is arbitrarily chosen and then divided into several vertical slices, as in figure 14, slices do not need to be the same width (Das & Sobhan, 2018).

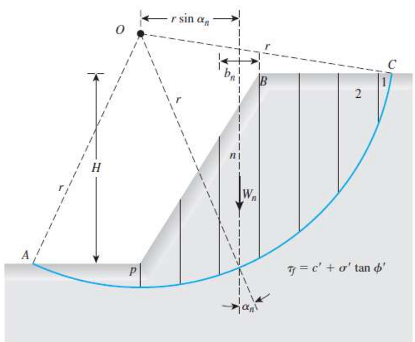

Figure 14 Dividing the slip into vertical slices (Das & Sobhan, 2018)

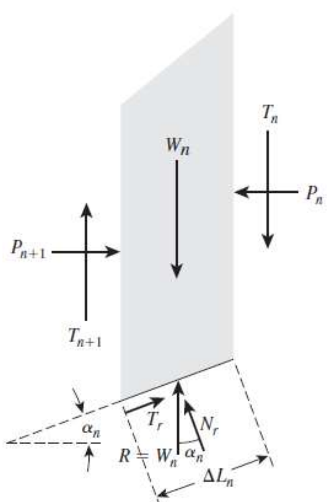

Figure 15 Single slice (Das & Sobhan, 2018)

The normal force can be expressed as $N_r = W_n cos\alpha_n$ where W_n is the weight of the slice and N_r the normal force, this is shown in figure 15 (Das & Sobhan, 2018).

The resisting shear force is represented by (Das & Sobhan, 2018):

$T_r = \tau_d(\Delta L_n) = \frac{\tau_f(\Delta L_n)}{F_s} = \frac{1}{F_s}[c' + \sigma' tan\emptyset']\Delta L_n$ which is equal to $\frac{N_r}{\Delta L_n} = \frac{W_n cos\alpha_n}{\Delta L_n}$ (Das & Sobhan, 2018).

Where τ_d is the developed shear stress, τ_f is the shear stress in the soil and σ' the normal stress.

Manipulating this we get (Das & Sobhan, 2018):

$$F_s = \frac{\sum_{n=1}^{n=p}(c'\Delta L_n + W_n cos\alpha_n tan\emptyset')}{\sum_{n=1}^{n=p}(W_n sin\alpha_n)}$$

Where:

c' = cohesion
$\emptyset'$ = internal angle of friction

2.1.1.2 Bishop's Simplified Method of Slices

The Bishop's method gives more refined results than the ordinary method of slices because the effects of the forces on the sides are accounted for to some extent (Das & Sobhan, 2018). The addition of these has however only a marginal effect on the factor of safety (Craig, 2004). It can be used where a wide range of different soil strata are present (Craig, 2004). It can only be used for circular slips and has numerical problems under some conditions (Duncan, 1996). The Bishop's method does not satisfy equilibrium with respect to forces, only moments (Das & Sobhan, 2018). This method also does not account for pore water pressure (Das & Sobhan, 2018). This method is most widely used and gives satisfactory results when used in computer programs (Craig, 2004; Das & Sobhan, 2018). This method underestimates the factor of safety (FOS) by a value that does not normally exceed 7% and normally is below 2% (Craig, 2004). Spencer showed that Bishop's simplified method of slices' accuracy is due to the insensitivity of the moment equation to the slope of the interslice forces (Craig, 2004).

When a numerical problem occurs in the Bishop's method, the factor of safety will be lower than the results from the ordinary method of slices, thus when the Bishop's method is used it should be compared to results from the ordinary method for comparison (Duncan, 1996).

In figure 16, T_n and T_{n+1} are the shearing forces and P_n and P_{n+1} normal forces that act on the sides of the slice, they are often approximated as $T_n = P_n$ and $T_{n+1} = P_{n+1}$ and, $\Delta T = T_n - T_{n+1}$ and $\Delta P = P_n - P_{n+1}$ (Das & Sobhan, 2018).

$$T_r = N_r(tan\emptyset'_d) + c'_d\Delta L_n = N_r\left(\frac{tan\emptyset'}{FOS}\right) + \frac{c'\Delta L_n}{FOS}$$

Where:

c' = cohesion
$\emptyset'$ = internal angle of friction

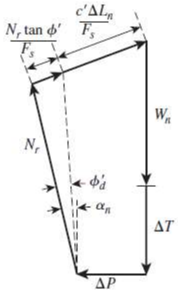

Figure 16 Force polygon of forces acting on nth slice for equilibrium (Das & Sobhan, 2018)

From the force polygon the following relation is gained (Das & Sobhan, 2018):

$$W_n + \Delta T = N_r cos\alpha_n + \left[\frac{N_r tan\emptyset'}{F_s} + \frac{c'\Delta L_n}{F_s}\right] sin\alpha_n$$

Which can be rearranged as:

$$N_r = \left(W_n + \Delta T - \frac{c'\Delta L_n}{F_s}\ sin\alpha_n\right) \div \left(cos\alpha_n + \frac{tan\emptyset' sin\alpha_n}{F_s}\right)$$

To calculate the factor of safety equilibrium is used by taking the moments around O which gives:

$$\sum_{n=p}^{n=p} W_n r sin\sigma_n = \sum_{n=p}^{n=p} T_r r$$

Where T_r can be substituted and then rearranged into:

FOS $= \frac{\sum_{n=p}^{n=1}(c'b_n + W_n tan\emptyset' + \Delta T tan\emptyset')\frac{1}{m_{\alpha(n)}}}{\sum_{n=1}^{n=p} W_n sin\ \ _n}$ and this can be simplified by taking $\Delta T = 0$.

Where:

$$m_{\alpha(n)} = cos\alpha_n + \frac{tan\emptyset' sin\alpha_n}{\text{FOS}}$$

2.1.1.3 Method of Slices for Steady-State Seepage

In the method of slices for steady-state seepage, the ordinary method of slices or Bishop's simplified method of slices is modified to account for steady-state seepage (Das & Sobhan, 2018). The pore water pressure (u_n) at the bottom of a slice is $u_n = h_n\gamma_w$, where h_n is the hight of water in the slice and γ_w is the water's density, and at the force caused on the n'th slice is $u_n\Delta L_n$ (Das & Sobhan, 2018).

The ordinary method of slices is modified as follow:

$$F_s = \frac{\sum_{n=1}^{n=p}\left(c'\Delta L_n + (W_n cos\alpha_n - u_n\Delta L_n)\right)tan\emptyset'}{\sum_{n=1}^{n=p}(W_n sin\alpha_n)}$$

And the Bishop's simplified method of slices becomes:

$$\text{FOS} = \frac{\sum_{n=p}^{n=1}(c'b_n + (W_n - u_n b_n)tan\emptyset')\frac{1}{m_{\alpha(n)}}}{\sum_{n=1}^{n=p} W_n sin\alpha_n}$$

2.1.1.4 Spencer's Solution

Spencer's solution satisfies equilibrium both in respect to forces, as well as moments (Das & Sobhan, 2018).

The same charts can be used as per the charts developed by Bishop and Morgenstern to determine the factor of safety, which is further discussed in the next heading (Das & Sobhan, 2018).

2.1.1.5 Morgenstern's Method of Slices for Rapid Drawdown Condition

Using the modified Bishop's simplified method of slices, Bishop and Morgenstern developed tables from which the factor of safety can be read off of for simple slopes after some preliminary calculations (Craig, 2004; Das & Sobhan, 2018). In this method the fact that the factor of safety varies linearly with the pore pressure ratio (r_u) is considered (Craig, 2004). The slope angle, internal angle of friction ($\emptyset'$), a depth factor and a dimensionless factor $c'/(\gamma H)$ is used to calculate two stability coefficients, m and n, which in turn is used to calculate the factor of safety ($FOS = m - nr_u$)(Craig, 2004). $c'/(\gamma H)$ is zero where the critical-state strength is used (Craig, 2004).

Important assumptions from Morgenstern was that the slope is of a homogeneous material, it rests on an impervious base, initially the water level is the same as the top of the embankment, pore water pressure does not dissipate with drawdown and that the unit weight of saturated soil (γ_{sat}) $= 2\gamma_w$, where γ_w is the unit weight of water (Das & Sobhan, 2018).

2.1.1.6 Morgenstern and Price Method

Note: In this section the symbols are used that corresponds to the symbols given by Craig (2004) and is different to the symbols used prior of after this section. They are:

E = effective normal force on a side of the slice, given as P_n in the previous sections
X = shear force on a side, given as T_n in the previous sections
P_w = boundary water force on a side
dN' = effective normal force on the base of the slide, the normal force symbol was N_r in the previous section.
dS = shear force on the base, the shear force on the base was given as T_f in the previous sections
dP_b = boundary water force on the base, not defined as a symbol but used in the previous sections
dW = total weight of the slice, the symbol for weight is the same as prior

The Morgenstern and Price method is readily available for use in computer programs, and is the most appropriate method to analyse embankment dams, due to its inherent accuracy (Craig, 2004). Because the upstream slope of an embankment dam is at a critical stage at rapid drawdown, and the Morgenstern and Price method deals with this well, it is also appropriate in that aspect (Craig, 2004).

In the Morgenstern and Price method, all the equilibrium and boundary conditions are satisfied and the failure surface may be circular, non-circular or compound (Craig, 2004). Similar to the other method of slices, an arbitrary slip is chosen and divided into several perpendicular vertical slices (Craig, 2004). This is then analysed where after a new slip is chosen to repeat the process.

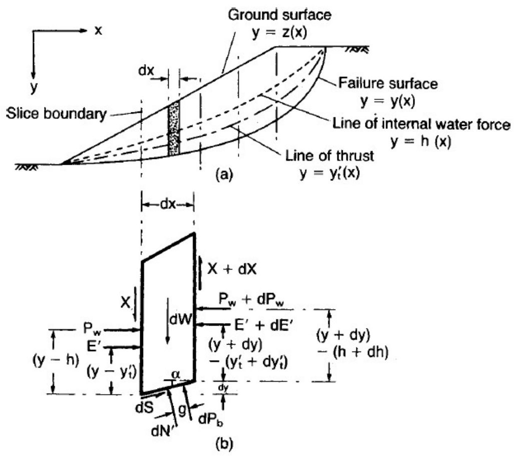

Figure 17 The Morgenstern-Price Method (Craig, 2004)

In figure 17, $y = h(x)$ represents the internal water forces (P_w) and $y = y'_t(x)$ the line of thrust of the effective normal force (*E')* (Craig, 2004). The moments around the mid-point of the base and the forces parallel and perpendicular to the base are separately equated to zero according to equilibrium, which is simplified by working in terms of the total normal force (*E*), where $E = E' + P_w$ (Craig, 2004).

The position of *E* is then obtained by: $Ey_t = E'^{y'}{}_t + P_w h$ (Craig, 2004). To make the problem statically determinate, a relationship is assumed of $X = \lambda f(x)E$ where λ is a scale factor and $f(x)$ represents the pattern of variation of the ration X/E (Craig, 2004).

The boundary conditions *E* and *M* are calculated at each end of the slip circle, both of which is normally equal to zero at these locations, by calculating the integral of the expressions containing *E* and *X* (Craig, 2004). First trail values are chosen for λ and F, E is set as zero at the beginning of the slip, and the each slice is then integrated in turn, resulting in values for E, X and y_t (Craig, 2004). The calculated value for *E* and *M* at the end of the slip is normally not equal to zero (Craig, 2004). This process is repeated by choosing new values for λ and F, E using the Newton-Raphson method until the *E* and *M* is equal to zero at both ends of the side (Craig, 2004). $f(x)$ is often taken as 1 because of the small effect it has on the factor of safety (Craig, 2004).

This method requires that the implied state of stress within the soil mass above the surface is checked to ensure that neither shear failure nor a state of tension is implied within the mass (Craig, 2004). This is important for all methods of slices, because deformation is not accounted for. The way in which this is done is by comparing the shearing resistance on each vertical interface with the value of the force *X* (Craig, 2004). The amount that the shearing resistance is greater than X represents a local factor of safety against shear failure (Craig, 2004). Also, if the line of thrust of force *E* lies above the failure surface, then no tension is developed (Craig, 2004).

2.1.1.7 Fellenius or Swedish Solution

This solution assumes that the resultant of all the interslice forces is equal to zero (Craig, 2004). This method is conservative (underestimates FOS) and has an error of 5-20% when compared to more accurate methods (Craig, 2004). This method is not recommended or used much in practice (Craig, 2004). All the forces are first resolved into forces normal to the base, $N_f = W cos\alpha - ul$ (Craig, 2004). This method, like all methods using force equilibrium, have numerical problems in some cases (Duncan, 1996).

The factor of safety is then calculated as follow (Craig, 2004):

$$\text{FOS} = \frac{c'^{L_a} + tan\emptyset' \sum_{n=p}^{n=1}(Wcos\alpha - ul)}{\sum_{n=p}^{n=1}(Wsin\alpha)}$$

2.1.1.8 Other methods of slices

Some of the other methods include a method proposed by Bell and one by Sarma (Craig, 2004). The method Sarma propose to evaluate the critical earthquake acceleration required to produce a condition of limiting equilibrium (Craig, 2004). In Bell's method the condition of equilibrium is satisfied and any shape can be used (Craig, 2004). Both these methods require the use of a computer (Craig, 2004).

2.1.2 Mass procedure/ Limit state method

The limit state method is normally used, where it is considered that a failure is on the point of happening along a known failure surface (Craig, 2004). Using the limit state method, the disturbing force must be less or equal to the design resisting force (Craig, 2004).

This method is most useful in homogeneous soils, even if this is not common in nature (Das & Sobhan, 2018). One of the major flaws of this method is that it is only applicable to slopes of saturated clay under undrained conditions ($\emptyset = 0$) (Das & Sobhan, 2018).

A slip circle is chosen arbitrarily and tested where it is assumed that the shear strength of the soil is constant with depth and is given by $\tau_f = c_u$ (Das & Sobhan, 2018). The slip is divided into two weights W_1 and W_2 (refer to figure 18), which represents the weight of the soil part of the slip (Das & Sobhan, 2018). These weights are multiplied by their lever arms l_1 and l_2 and the difference between these moments is the driving moment (M_d) for the slip (Das & Sobhan, 2018).

$$M_d = W_1 l_1 - W_2 l_2$$

The resisting moment (M_R) is derived from the cohesion acting on the potential sliding surface developed cohesion (c_d) (Das & Sobhan, 2018).

$$M_R = c_d(sliding\ surface)(1)(r) = c_d r^2 \theta$$

For the material to be in equilibrium $M_d = M_R$ and thus $W_1 l_1 - W_2 l_2 = c_d r^2 \theta$ which can be rearranged as $c_d = \frac{W_1 l_1 - W_2 l_2}{r^2 \theta}$ (Das & Sobhan, 2018).

The factor of safety is then found by $FOS = \frac{\tau_f}{c_d} = \frac{c_u}{c_d}$ (Das & Sobhan, 2018).

The critical surface is where the ratio of c_u and c_d is at a minimum (Das & Sobhan, 2018). This process is repeated with new slip circles until the lowest factor of safety is achieved, which is then adopted as the factor of safety for the slope (Das & Sobhan, 2018). Of note is that the circle does not always go through the toe of the slope (Das & Sobhan, 2018).

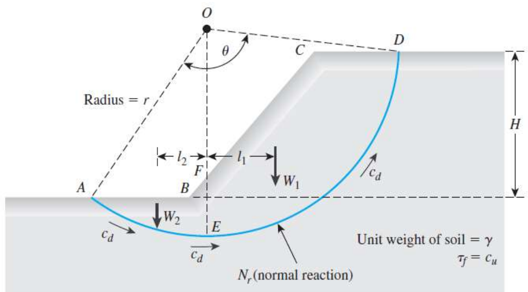

Figure 18 Mass procedure (Das & Sobhan, 2018)

c_d can also be expressed by $c_d = \gamma H m$ where m is the stability number and different values of this can read of a graph developed by Terzaghi and Koppula has introduced values of m and an additional horizontal force that account for earthquakes (Das & Sobhan, 2018). For the critical height $FOS = 1$ and the height (H) can be substituted by the critical height (H_{cr}) and c_d by c_u (Das & Sobhan, 2018).

2.1.3 Numerical methods

Numerical methods can be used where loadings are not static, complex geometries need to be assessed, deformation is assessed or strain needs to be considered (Bobet, 2010). The two classifications for numerical methods are continuum and discontinuum methods (Bobet, 2010). In discontinuum methods, the discontinuities are incorporated explicitly, while in the continuum methods discontinuities may be incorporated implicitly or explicitly (Bobet, 2010). The choice of method would be dependent on size or scale of the discontinuities with respect to the size or scale of the problem that needs to be solved (Bobet, 2010).

The Continuum methods include Finite Difference Method (FDM), Finite Element Method (FEM), Finite Volume Method (FVM), and the Boundary Element Method (BEM) (Bobet, 2010). The Discontinuum methods includes the Distinct Element Method (DEM), Discontinuous Deformation Analysis (DDA) and the Bonded Particle Method (Bobet, 2010).

2.1.4 Numerical methods - Continuum methods

In FEM and FDM, the medium and boundaries are discretized and in BEM the boundaries are discretized (Bobet, 2010).

2.1.4.1 Finite differencing method

FDM is the predecessor to the other numerical methods and has a history dating back before the use of computers (Bobet, 2010). In this method the differential equations are reduced to a system of linear equations which are solved using classical methods (Bobet, 2010). The method can also be employed to evaluate dynamic problems, and can model non-linear behaviour well (Bobet, 2010).

In FDM a grid is superimposed onto a domain, as per figure 19, that requires evaluation, and approximation of the field equations are used then to perform the analysis (Bobet, 2010). Discontinuities are accounted for by evaluating points on either side of the discontinuities (Bobet, 2010). The friction laws (e.g. Coulomb) is used and this is reinforced with equations that relate shear stress with normal stress (Bobet, 2010). The displacement between grid points are used to determine the slip along discontinuity (Bobet, 2010). Shear and normal stiffness of the discontinuity can also be obtained from the normal and shear displacement (Bobet, 2010).

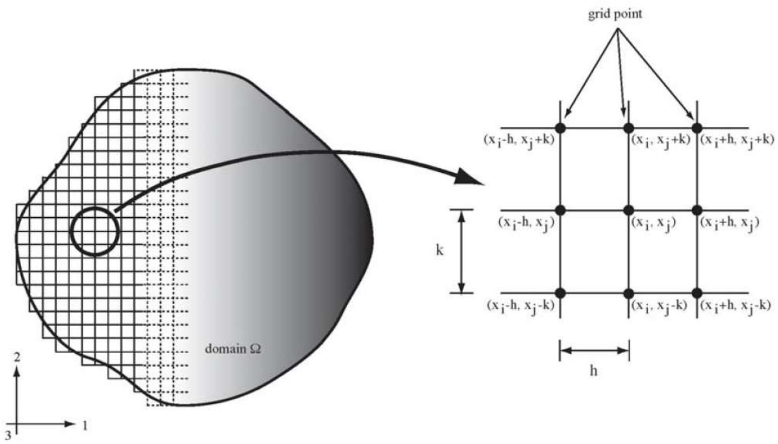

Figure 19 FDM grid in 2D (Bobet, 2010)

Dynamic problems are solved by increasing the timestep to the maximum available and is given by (Bobet, 2010):

$$\Delta t = min\left(\frac{\Delta x}{C_p}\right)$$

$$C_p = \sqrt{\frac{K + 4/3G}{\rho}}$$

C_p = Compressional or P-wave velocity in soil
$\Delta x =$ Grid spacing
$K =$ Bulk modulus
$G =$ Shear modulus
$\rho =$ Density of soil

The timestep is controlled by the stiffness of the material, and may be tens of thousands, but the memory required to store a solution is small (Bobet, 2010). Complex problems can be completed in a fair time (Bobet, 2010). The solution is done in small steps where the displacement is gained after each step (Bobet, 2010). The stresses gained at each grid point is then used to update the stress field from the previous increment (Bobet, 2010). This method is a forward scheme and does not require iterations (Bobet, 2010).

2.1.4.2 Finite Element Method

Finite Element Methods have been used in geotechnical evaluations since the 1950s (Craig, 2004). They can be used for various analyses, including those that are complicated (Craig, 2004; Das, 2011). It is the most common method used for continuous or quasi-continuous material (Bobet, 2010). It has also been used to successfully calculate pore water pressure, movement, deformations and stresses in slopes (Duncan, 1996). Finite element methods provide a method to model geotechnical conditions with a high degree of realism (Duncan, 1996).

Finite element methods help identify potential deformations and stresses within an embankment, which cannot be done with limit equilibrium methods (Craig, 2004). Progressive failures can also result from the stress-strain characteristics, and thus needs to be evaluated (Craig, 2004). By evaluating these stress and strain relationships finite element programs can predict cracking, due to differential movement between soil zones, and fractures (Craig, 2004; Duncan, 1996). Potential fracturing, like hydraulic fracturing where the total normal stress is less than the local value of pore water pressure, can also be considered (Craig, 2004). But, finite element analysis are often quite expensive, time consuming, requires specialized training and high-end computing resources, which is not always practical (Das, 2011; Duncan, 1996).

Finite element method is based on the principle of virtual displacement, which states that when a body is in equilibrium, the total internal work required for any small virtual displacement that satisfies the boundary conditions (compatible), is equal to the total virtual external work (Bobet, 2010). Thus, the displacement of any point in an element, can be obtained by calculating the displacement of the corresponding node, by using the appropriate interpolation function (Bobet, 2010). In finite element method, discretization of the domain into small elements that intersect at nodes takes place first, see figure 20 (Bobet, 2010). When modelling the construction of an embankment or an excavation about eight layers are needed in the grid used, even though sufficient accuracy can sometimes be achieved with fewer layers (Duncan, 1996). The number of steps needed is a function of the height/depth of the embankment/excavation (Duncan, 1996).

Then, a set of differential equations are translated into a matrix equation for each element, and relating forces at nodes into displacements at nodes (Bobet, 2010; Itasca Consulting Group, 2017a). These differential equations has the following as inputs: initial conditions, stress-strain, and loading sequence, or where existing fills are evaluated, the initial stress is required (Duncan, 1996). Incremental analysis is preformed to realistically simulate field conditions (Das, 2011). These field conditions include; nonlinear stress-strain behaviour, changes in geometry, and sequential changes in excess pore water pressure with progress, and type of construction (Das, 2011). The natural slope, temperatures, consolidation, and water table needs to be modelled as accurately as possible (Duncan, 1996). The biggest contribution that finite element methods brought to geotechnical evaluations, is the ability to assess nonlinear stress-strain behaviour (Duncan, 1996).

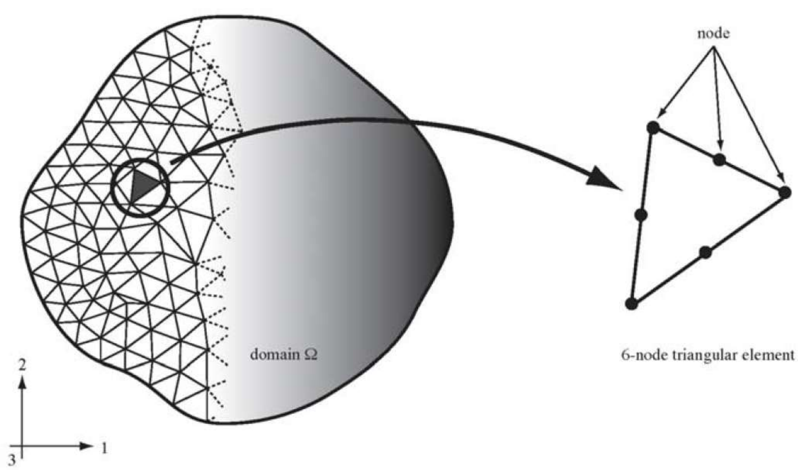

Figure 20 Two Dimensional Finite Element Discretization (Bobet, 2010)

For the inputs, the initial stresses are first obtained (Duncan, 1996). This is normally estimated, even though it can be measured, and the vertical stresses are taken as the overburden pressure and the horizontal stresses as k_0 times the overburden pressure (Duncan, 1996). k_0 is normally estimated using an empirical relationship (Duncan, 1996). For non-level ground, the stresses will be greater, and a gravity turn-on analysis can be used (Duncan, 1996).

The reference state for stresses is chosen to satisfy equilibrium (Duncan, 1996). The reference state for displacement can be chosen arbitrarily, but needs to be used consistently, and is often chosen as zero

(Duncan, 1996). Because the reference state for strain can also be chosen arbitrarily, the non-linear stress-strain relationship is related to stresses (Duncan, 1996).

The stress-strain plays an important role, and where the strains are small the soil can be represented as an elastic material (Duncan, 1996). Mostly though, it accounts for non-linear behaviour which accounts for the soil modulus values varying with the confining pressure (Duncan, 1996).

2.1.4.3 Boundary Element Method (BEM)

The boundary element method is well-suited for problems where a small boundary to volume ratio is present, the continuum is static, elastic behaviour is present, and stresses or displacement is applied to the boundaries (Bobet, 2010). This is method is not always practical because in many cases, yielding may occur under moderate stresses, gravity may be significant, and inertia may play an important role with dynamic loading (Bobet, 2010).

In the boundary element method the boundary is discretized of the continuum opposed to the entire medium, see figure 21 (Bobet, 2010). In BEM no artificial boundaries are needed opposed to FDM and FEM, which means that the medium can extent to infinity, which is common for problems in geomechanics (Bobet, 2010). The solution are approximated at the boundary and exactly satisfied in the interior whereas in FDM and FEM the approximation is inside the medium (Bobet, 2010).

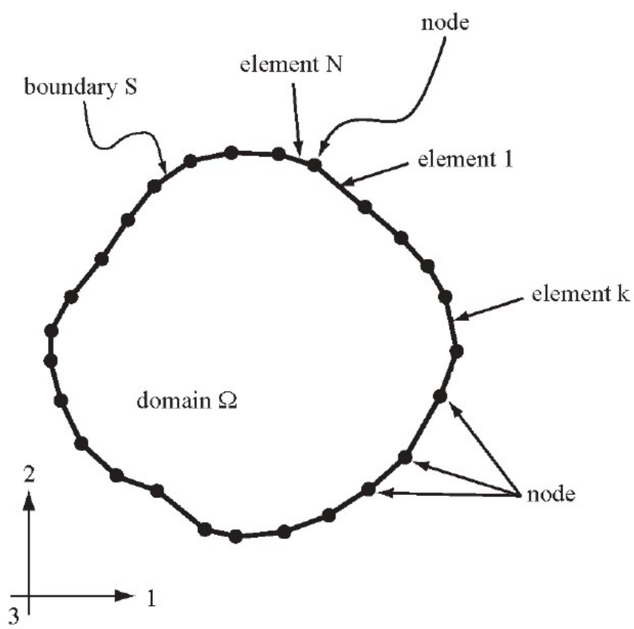

Figure 21 Two-dimensional Discretization with Boundary Element Method (Bobet, 2010)

In this method the differential equations are integrated which will then only apply to the boundary values (Bobet, 2010). This technique is attractive where large volumes exist, because it reduces the problem by one order by limiting the discretization to the boundaries, thus from 3D to 2D and from 2D to a line (Bobet, 2010). The unknown parameter can be solved either through direct BEM or indirect BEM. In direct BEM the stresses and displacement are calculated and are then known parameters which is then used to calculate the displacement and stresses elsewhere in the medium. When the indirect method is used, fictional values are given to either the stresses or displacement, and then the other stresses and displacement elsewhere in the medium is then given in terms of this fictional value (Bobet, 2010).

The advantages of BEM will be lost when plastic deformation, dynamic or body forces are evaluated, because this requires integration over the entire volume, which need discretization of the entire continuum (Bobet, 2010).

2.1.4.4 Finite volume method

FLAC3D uses the strength reduction method and the Lagrangian formula. These are applied using methods based on the finite volume method (Itasca Consulting Group, 2017a). In the finite volume method, the divergence theorem is used to convert partial differential equations to surface integrals.

FLAC3D is based on the motion equations, time stepping, and an explicit scheme (Itasca Consulting Group, 2017a).

In the strength reduction method the Mohr-Coulomb failure criterion is often used (Itasca Consulting Group, 2017b). The Mohr-Coulomb states that a material fails because of the critical combination of normal and shear stress (Das & Sobhan, 2018). This method allows for analysis of various geotechnical structures, not all of which is has circular, log spiral or plane patterns (Das, 2005). Also, unlike the other methods deformation can also be assessed, and thus it covers the other some of the other failure mechanisms, which include fall, topple, or spread (Craig, 2004). The Mohr-Coulomb failure criterion is expressed as follows (Das, 2005):

$$\tau_f = c + \sigma\, tan\emptyset$$

Where:

τ_f = shear stress on the failure plane
c = normal stress on the failure plane
σ = cohesion
$\emptyset$ = angle of internal friction

In the strength reduction method, the shear strength is reduced until a state of equilibrium occurs (Ma, Su, & Li, 2020). The strength reduction factor (SRF) that causes failure, is the factor of safety (Ma et al., 2020). FLAC3D either reduces the cohesion and friction angle until failure occurs or, where the slope starts to fail, it increases these until a stable slope is obtained (Itasca Consulting Group, 2017b). The equations for the factor of safety in FLAC3D is as follows (Ma et al., 2020):

$$c = c'/SRF$$

$$\emptyset = \arctan\,(tan\emptyset'/SRF)$$

Where:

c = cohesion
$\emptyset$ = internal angle of friction

The strength reduction method is often used in numerical methods, using finite element design software packages, and can be used to draw a plane strain model (Knight, 2015; Meisheng & Laigui, 2011). These programs come in 2D and 3D variations (Shen et al., 2012).

FLAC3D uses a strength reduction method to obtain the factor of safety (Itasca Consulting Group, 2017b). FLAC3D can also model motion and deformation which is opposed to the steady state analysis provided by other programs (Itasca Consulting Group, 2017b). Like other finite difference or finite element techniques, modelling of complex slope topography requires large amount of effort in pre-processing (Shen et al., 2012). This said, 3D analysis reduces the subjective nature of selecting the weakest area, and gives less conservative factors of safety than 2D analysis (Shen et al., 2012). Even with the increase of processing time, a 3D analysis is more appropriate for assessing relative important slopes (Shen et al., 2012). Numerical methods, though programs like FLAC3D, are not always used, because of the comparatively difficulty of drawing these models, compared to limited equilibrium models (Shen et al., 2012).

2.1.4.5 Determining the stress-strain relationship

The method can be based on either plasticity or elastic theory (Duncan, 1996). Plasticity theory will be used where undrained analysis is required in terms of effective stresses and is used to model changes in pore water pressure resulting from loading (Duncan, 1996). Also, it is used on local failures where the behaviour is controlled by properties of materials that have already failed (Duncan, 1996). In these, elastic theory has significant shortcomings (Duncan, 1996). Linear Elastic analysis are simple to do because they only require Young's modulus (E) and Poisson's ratio (v), but they are not good at modelling actual stress-strain behaviour in soil (Duncan, 1996). Linear elastic analysis only works well where low stress levels and small strains are present, and can give reasonably accurate results where there are not zones of strongly differing stiffness (Duncan, 1996). There is no single rational way to select a value for Young's modulus or Poisson's ratio, because they are dependent on the confining pressure and deviator stress (Duncan, 1996).

Other methods include multilinear elastic, hyperbolic elastic, elastoplastic and elastoviscoplastic (Duncan, 1996). Multilinear elastic increases the accuracy of the stress-strain curve by adding more lines in an ad-hoc manner (Duncan, 1996). This allows for a reduction in modulus while increasing strain (Duncan, 1996). This method results in good results but overestimates movement (Duncan, 1996). This overestimation can be attributed to (Duncan, 1996);

- the remoulding required in the lab resulting in less stiff material,
- in-situ material that is often more densely compacted,
- triaxial tests which are mostly used, tend to produce lower sloped stress-strain curves as opposed to what in-situ material has, which is closer to plain-strain,
- and in valleys 2D analysis does not take into account cross valley arching.

Hyperbolic elastic stress strain relationships use Hooke's Law to relate strain increments to stress increments (Duncan, 1996). The use of hyperbolic curves can be determined by conventional laboratory tests and are widely used (Duncan, 1996). The best way to obtain a value for Poison's ratio, is determined by relating the bulk modulus to the mean normal stress (Duncan, 1996). Selecting a single value logically is difficult because of its dependence on stress conditions (Duncan, 1996). Also, where a soil has failed and a small modulus is assigned to represent the soil having reached the top of the stress-strain curve, the model would show that the soil is not able to resist any type of strain, which is not true (Duncan, 1996). Poison's ratio can also be determined by relating it to the confining pressure and deviator stress, but this method has problems under some conditions (Duncan, 1996).

Where a situation exists in which a failure is imminent, more complex methods to determine the stress-strain may be justified (Duncan, 1996). This can be done through either elastoplastic or elastoviscoplastic methods, giving better results (Duncan, 1996). The main difference in these methods is at high stress situations (Duncan, 1996). Elastoplastic methods are especially useful where undrained conditions are analysed in terms of effective stresses, but this is highly dependent on the accuracy of the changes in pore pressures caused by changes in total stress (Duncan, 1996). At low stress levels these methods do not produce significantly better results than nonlinear elastic stress-strain relationships (Duncan, 1996).

2.1.5 Numerical methods - Discontinuum methods

2.1.5.1 Distinct element method

The distinct element method (DEM) is used to model granular material (Zhao, Xu, Youhu, Zhang, & Ciao, 2018). DEM has been extensively validated and is very versatile (Bobet, 2010). It can be used in full three-dimensional problems and can be applied to deformable bodies and fragmentation of discontinua by discretizing the elements with finite element or finite difference meshes, as shown in figure 22 (Bobet, 2010). Pre-existing joints in rock can be incorporated directly and they are allowed to undergo large deformations (Bobet, 2010). DEM is used for both static and dynamic calculations (Bobet, 2010).

Discrete bodies are allowed to displace, rotate or detach and make new contacts during calculation (Bobet, 2010). The domain is divided into blocks interconnected through discontinuities (Bobet, 2010). Each block is subject to its internal forces and the forces applied by the surrounding forces (Bobet, 2010).

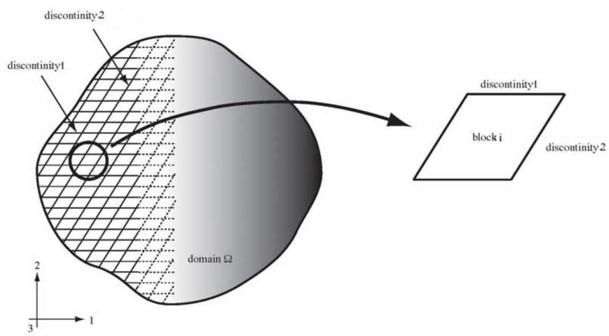

Figure 22 DEM and DDM Discretization (Bobet, 2010)

The process of calculation using DEM is as follows; calculations are started at a fully known state and done to an unknown state, firstly Newton's second law is used to determine the relevant displacement and velocities at the contact between elements (Bobet, 2010). This is used to determine the contact forces which in turn is used to determine the resultant force and moments at the centre of gravity of each block (Bobet, 2010). This is repeated thousands of times using either real or fictional timesteps that are very small until a final solution is obtained (Bobet, 2010). The timesteps need to be smaller than the critical timestep which is given as (Bobet, 2010):

$$\Delta t_{crit} = \kappa \sqrt{\frac{m_{min}}{2K_{max}}}$$

Where:

κ = factor to account for multiple contacts and is suggested as 0.1
m_{min} = smallest element mass
K_{max} = largest normal or shear stiffness

DEM doesn't require a lot of time to run or a lot of storage except to keep track of all the contacts (Bobet, 2010).

Newton's second law is used to define the displacement of the blocks and the equations are given as follows (Bobet, 2010):

$m\ddot{u}_i^t + c\dot{u}_i^t = F_i^t$ and $I\dot{\omega}^t + c\omega^t = M^t$

Where:

t = time
m = mass
I = moment of inertia
u_i = displacement of the gravity center of the element in the direction i
$\ddot{u}_i$ = acceleration of the gravity center
$\dot{u}_i$ = velocity of the gravity center
ω = angular rotation of the element
$\dot{\omega}$ = angular velocity of the element
c = viscous damping
F_i = resultant force applied to the center of gravity
M = moment applied at the center of gravity

These equations are solved using a finite difference method (Bobet, 2010). A penalty method can be used to obtain the shear and normal forces that exists between blocks (Bobet, 2010). The movement along the direction of contact between blocks, is proportional to the shear stress and the movement along the normal direction, is proportional to the normal force. (Bobet, 2010) The expressions are as follows (Bobet, 2010):

$$F_n^{t+\Delta t} = F_n^t - K_n \Delta u_n^{\Delta t} A_c - \beta K_n \Delta \dot{u}_n^{\Delta t} A_c$$

$$F_s^{t+\Delta t} = F_s^t - K_s \Delta u_s^{\Delta t} A_c - \beta K_s \Delta \dot{u}_s^{\Delta t} A_c$$

Where:

K_n = normal stiffness
K_s = shear stiffness
Δu_n = relative displacement
Δu_s = relative displacement
A_c = contact area
β = damping factor

The shear force is limited by a Coulomb-type friction law against which it is tested as a limiting factor (Bobet, 2010):

$$F_s^{t+\Delta t} \leq cA_c + F_n^{t+\Delta t} tan\emptyset$$

Where:

c = cohesion
$\emptyset$ = friction angle of the contact area

2.1.5.2 Discontinuous Deformation Analysis (DDA)

DDA is also used for large grained materials and can be used to solve both 2 dimensional and 3 dimensional problems (Bobet, 2010). It allows for fragmentation and fracture propagation problems and the method has been validated (Bobet, 2010).

When applying DDA to two dimensional problems, discretization of a domain into blocks is fundamentally the same for DDA as per DEM and figure 22 can also be used (Bobet, 2010). Blocks are represented by polyhedra in three-dimensional analysis and the shape is determined by their location and contacts with neighbouring blocks (Bobet, 2010). There are no penetration of, or tension between elements allowed and this is attained by adding “springs” between elements (Bobet, 2010). In DDA the total potential energy of the system is minimized to find a solution, and the displacements are unknown at the start (Bobet, 2010). DDA uses an explicit method and the procedure resembles FEM (Bobet, 2010).

Large deformations can be represented by a sufficient amount of small deformations and in 2D the following formulas can be iterated to calculate the strains (Bobet, 2010):

$$u = u_0 + (x - x_0)a_1 + (y - y_o)a_2$$

$$v = v_0 + (x - x_0)b_1 + (y - y_o)b_2$$

Where:

u and v = displacement on the x and y-axis
u_0 and v_0 = rigid body motions at point x_0 and y_0
a_1, a_2, b_1 and b_2 = constants

Displacements are then calculated from the strain as follow (Bobet, 2010):

$$u = u_0 + (x - x_0)\varepsilon_{xx} + (y - y_o)\left(\frac{1}{2}\gamma_{xy} - r_0\right)$$

$$v = v_0 + (y - y_0)\varepsilon_{yy} + (x - x_o)\left(\frac{1}{2}\gamma_{xy} - r_0\right)$$

Where:

ε_{xx}, ε_{yy} and γ_{xy} = axial strains and shear strains in the x and y-axis
r_0 = rigid element rotation in radian

These can be expressed in to the matrix notation U = TD where U = (U,v), $D^T = (u_0, v_0, r_0, \varepsilon_{xx}, \varepsilon_{yy}, \gamma_{xy})$ and T is the appropriate coefficients from the strain calculations (Bobet, 2010). The strain in in each element is constant and there are 6 degrees of freedom (Bobet, 2010). Thus, for N elements there are 6N unknowns (Bobet, 2010).

The following FEM convention is used to minimize the potential energy of the system of elements (Bobet, 2010):

$$K_{ij}D_j = F_i$$

K_{ij} is a 6x6 and D_j a 6x1 matrix (Bobet, 2010).

To solve a system using DDA, the equations of equilibrium is used with a fictional system of springs (Bobet, 2010). These springs can be locked in a direction to allow for tension between two elements by stiffening the springs (Bobet, 2010). Once the spring is unlocked, the elements can separate (Bobet, 2010). This adding and removing of springs prevents penetration, and these springs are added and removed through an iterative process until all the kinematic constraints are satisfied (Bobet, 2010). The original threshold distance between elements is established during the definition of the elements, where after contacts are checked (Bobet, 2010). After each iteration the new position of each element is updated and if interpenetration is detected, locks are applied and if the relative distance is lower than the their initial distance, no contact check is done (Bobet, 2010). The equilibrium equations are used to determine interpenetration, and stiff springs are added with each iteration until no interpenetration occurs (Bobet, 2010). The spring forces are calculated and used to determine forces normal to the contact area, and if they are tensile, the normal spring is removed (Bobet, 2010). If the parallel component of the force is larger than the maximum allowed as given per Coulomb ($F_s > \mu F_n$), sliding is allowed by adding a spring in the normal direction (Bobet, 2010). If the force is smaller than allowed, springs in both directions are added (Bobet, 2010).

2.1.5.3 Bonded Particle Method

The bonded particle model has been used for; slope stabilities, evaluating the strength of rock materials, in tunnels to evaluate damage to rock masses, to evaluate supports, fracture mechanics, evaluating granular materials and for blasting and other dynamic analyses (Bobet, 2010).

The bonded particle method divides the domain into spheres or circles (discs) of different sizes, depending on whether 2- or 3-dimensional analysis is done, see figure 23 (Bobet, 2010). The discontinuum represents an agglomerate of cemented particles. Deformation is produced by the movement of these particles, and tensile or shear cracks when the tensile or shear strength of the contracts are reached (Bobet, 2010).

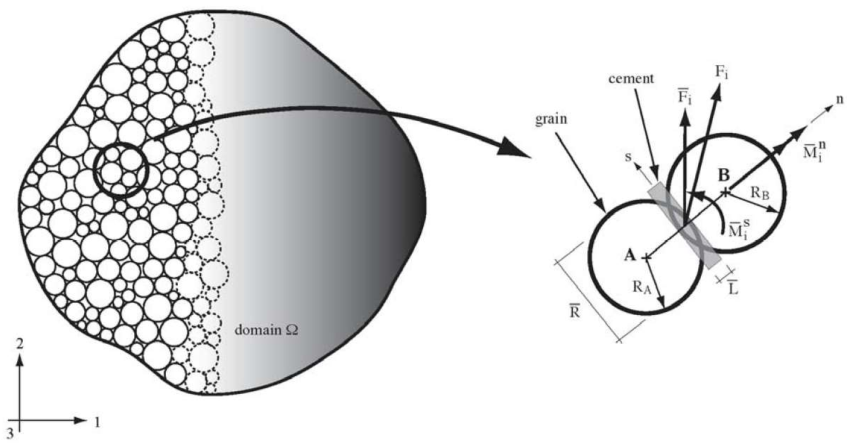

Figure 23 Discretization of Bonded Particle Method (Bobet, 2010)

A central finite difference algorithm uses the forces acting on the particles to solve Newton's second law of motion, through which displacements and velocities of each particle is solved (Bobet, 2010). The forces used are created by gravity for each particle and their interactions (Bobet, 2010).

The motion of the particle is determined in the same way that it was calculated using DEM (Bobet, 2010). Very small timesteps are used to incrementally apply static and dynamic loadings (Bobet, 2010). The forces and moments acting between particles is obtained though evaluating the relative motions between particles which is gained from the absolute displacement (Bobet, 2010). This is updated in the model, contacts reviewed and updated, and used for calculation in the next time-step (Bobet, 2010). This is repeated until a full solution is obtained (Bobet, 2010). The forces and moments, as per figure 23, acting on the particles are given by (Bobet, 2010):

$$F_i = F_i^n \vec{n} + F_i^S \vec{s}$$

$$\overline{F}_i = \overline{F}_i^n \vec{n} + \overline{F}_i^S \vec{s}$$

$$\overline{M}_i = \overline{M}_i^n \vec{n} + \overline{M}_i^S \vec{s}$$

Where:

F_i = interparticle forces
$\overline{F}_i^n$ and $\overline{F}_i^S$ = normal and parallel component of the interparticle force
$\overline{F}_i$ = force carried by the bond between the particles
$\overline{M}_i$ = moment carried by the bond between the particles

The magnitude of the loads are (Bobet, 2010):

$$\Delta F_i^n = \frac{k_n^A k_n^B}{k_n^A + k_n^B} \Delta U^n$$

$$\Delta F_i^s = -\frac{k_s^A k_s^B}{k_s^A + k_s^B} \Delta U^s$$

$$\Delta \overline{F}_i^n = \overline{k}_n A \Delta U^n$$

$$\Delta \overline{F}_i^s = -\overline{k}_s A \Delta U^s$$

$$\Delta \overline{M}^n = -\overline{k}_s J \Delta \theta^n$$

$$\Delta \overline{M}^s = -\overline{k}_n I \Delta \theta^s$$

$$A = \begin{cases} 2\overline{R} & in\ 2D \\ \pi \overline{R}^2 & in\ 3D \end{cases}$$

$$I = \begin{cases} \frac{2}{3}\overline{R}^3 & in\ 2D \\ \frac{1}{4}\pi \overline{R}^4 & in\ 3D \end{cases}$$

$$J = \begin{cases} n/a & in\ 2D \\ \frac{1}{2}\pi \overline{R}^4 & in\ 3D \end{cases}$$

Where:

k_n^A, k_S^A, k_n^A and k_n^B = normal and shear stiffness of particle A and B
ΔU^s and ΔU^n = Incremental normal and shear displacement between particles
$\Delta \theta^n$ and θ^s = incremental rotation angles in the normal and shear directions
A = Area of contact
I = moment of inertia
J = polar moment of inertia
$\bar{R}$ = bond radius

The shear and tensile stresses acting at the bond are:

$$\bar{\sigma}_{max} = -\frac{\overline{F}_i^n}{A} + \frac{|\overline{M}_i^s|\overline{R}}{I}$$

$$\bar{\tau}_{max} = -\frac{|\overline{F}_i^s|}{A} + \frac{|\overline{M}_i^n|\overline{R}}{J}$$

Where:

$\bar{\sigma}$ = tensile strength
$\bar{\tau}$ = shear strength

The bond between the particles are broken when the bond shear or tensile strength reaches the ultimate tensile or shear strength (Bobet, 2010).

The shear forces of the particles are limited by the constitutive law (Coulomb) (Bobet, 2010). When the displacement is negative, the particles move away from each other and there are no normal and shear forces, but when the displacement is positive, shear and normal forces occur (Bobet, 2010).

2.1.6 Experimental slope stability approaches

Other methods exist and include the use of probabilistic analysis methods or a combination of methods (Knight, 2015). Knight (2015) categorizes stability analysis methods in deterministic and problematic approaches. Deterministic methods include design charts and limited equilibrium methods (Knight, 2015). Problematic analysis used methods involving risk assessment techniques, like the Monte-Carlo analysis (Knight, 2015). Knight (2015) stated that many of the failures can be attributed to the use of deterministic methods of analysis, where many of the unknowns are not considered, which warrants a more holistic analysis but does not give proof of this.

Lin et al. (2018) looked at the applicability of using 4 different supervised learning algorithms. They found this should not be used blindly, because none of the 4 learning algorithms gave satisfactory results (Lin et al., 2018). Bobet (2010) gives a similar warning when describing Artificial Neural Network used for geological evaluations. He states that there is no way to be sure that the solution is correct because the methods used cannot be validated and solutions are given even when faults appear in the base assumptions.

2.1.7 Two-dimensional vs Three-dimensional analysis

It is generally given that two-dimensional approach gives more conservative results when compared to three-dimensional analysis (Das, 2011). This said, some would advocate that careful selection of a 2-D section will give comparable results to a 3-D analysis, even in complicated scenarios (Das, 2011). This selection of a most critical slope in 2-D analysis is where the problem arises, as a wrong one can be selected even where the highest slope is selected (Das, 2011).

Three-dimensional approaches are particularly useful where complex geometry, unusual distribution of shear strengths and/or pore water pressure within the potential sliding mass is present (Das, 2011). Three-dimensional approaches are also more appropriate for translational failures through underlying weak materials and/or geosynthetic interfaces (Das, 2011).

3-D analysis are heavily dependent on the accurate determination of shear strength, pore pressure, and field drainage conditions that can be challenging and this can in-turn reduce the accuracy of this compared to a 2-D analysis (Das, 2011).

2.1.8 Seepage and slope stability

When analysing the stability of an ash dam, a seepage analysis is sometimes coupled with a slope stability analysis (Li, Zhao, Chen, & Yang, 2005; Verdeș, 2017). As with other earth dams, programs like Slope/W and FLAC3D can be used to perform this (Verdeș, 2017).

Under normal circumstances toe-drains are installed in an ash dam (Li et al., 2005; Verdeș, 2017). This prevents seeping through the wall above the toe. This seepage above the toe is seen as a failure, because of the accompanying erosion (Ozcan et al., 2013). Thus, stability analysis do not normally consider seepage lines that daylight through the wall above the toe. Verdeș (2017) took the blockage of toe-drains as an extreme case and Li et al. (2005) did not consider it at all. Neither considers a situation where no toe-drains were installed.

2.1.9 Other factors affecting stability

The stability of a tailings dam can be altered by changing the slurry viscosity, depth of each lift (rate of rise), and the drying period (Knutsson, 2015). The inputs into a stability analysis of a tailings dam is; the internal angle of friction, specific gravity, pore water ratio, slope height, slope inclination and cohesive forces within the material (Craig, 2004; Das & Sobhan, 2018; Knight, 2015; Meisheng & Laigui, 2011). Other factors include the hydraulic regime of the dam, and the degree of compaction (Knight, 2015).

Failures are commonly caused by changes in permeability, changes in the phreatic surface, settlement of the foundation, ground vibrations, or steep slopes (Knight, 2015).

The destructive force of seepage and actual- versus theoretical phreatic levels need to be verified (Meisheng & Laigui, 2011).

2.1.10 Methods Used to Assess Slope Stability in Tailing Dams

The most common method of evaluating tailings and ash dams is through the 2-dimensional limit equilibrium methods and through numerical methods. Ozcan et al. (2013) showed that 2-dimensional limit equilibrium methods and numerical methods, in the form of FEM, show good agreement but did not evaluate a failure where a bi-planar failure mode was critical. He completed both dynamic and static evaluations.

Knight (2015) showed that stability charts and limit equilibrium methods using Slope/W gave comparable results and are all indicative of stability. Numerous others have solely used two-dimensional limit equilibrium methods (Karakuş, Özdoğan, Turan, Konak, & Onur, 2018; Li et al., 2005; Slávik, 2013; Slavik & Skvarka, 2019; Verdeș, 2017). Verdeș (2017) also used FEM, through using Seep/W, to solve the seepage part of his slope stability evaluation.

It is important to select the most dangerous section when using any two-dimensional method. When comparing the Lattice method and Exhaustion method to attain a most critical section the Lattice method is quicker and gives smaller results and is thus the preferred method (Li et al., 2005). In the evaluations by Li et al. (2005) he assumed that the critical slip circle will pass intersect near the toe of the slope.

Using FDM to evaluate tailing dam slopes gives satisfactory results for both static and dynamic cases, even where seepage is present (Meisheng & Laigui, 2011; Shen et al., 2012). Alternatively FEM can be used to evaluate the factor of safety for both static and dynamic cases where pore water is present in tailings dams (Knutsson, 2015; Rai, Khandelwal, & Jaiswal, 2011; Shen et al., 2012).

When comparing geotechnical parameters from triaxial and direct shear tests, the direct shear tests give more conservative results and is recommended even though the triaxial test results better correspond with site observations (Knutsson, 2015).

Building a three-dimensional model to be used in software packages like FLAC3D, can be difficult (Xu, Tian, Kulatilake, & Duan, 2011). Xu et al. (2011) proposed building a Sealed geological model using SGM with many topological and continuous connected blocks, by first constructing a wire frame and then tracing blocks. A tetrahedral mesh is then generated in each block and refined. Direct interpolation with dispersed data was used to simulate the interfaces of strata and fault lines into planes. The model is refined and imported to FLAC3D for analysis.

Shen et al. (2012) found, using the Mohr-Coulomb criteria, that three-dimensional analysis using FLAC3D gave 20-30% lower values than its 2D counterparts, and recommends 3D methods for complex and critical slopes.

2.2 Geotechnical evaluation

Commonly a stability analysis will start with a geotechnical investigation which may include a geological survey (Das & Sobhan, 2018). As part of the geological survey, soil samples are normally sent to a laboratory for analysis (Knutsson, 2015).

Validation of the properties gained from the laboratory can be done through simulations. Here results can be compared with field measurements through back analysis (Knutsson, 2015). One can guess properties and then see how models correspond to the actual behaviour of the material in question (Knutsson, 2015). One can also use deformation analysis to assess stability, but both these methods require large amount of effort and are not commonly used (Knutsson, 2015).

Where the cohesion of the soil is low, undrained geotechnical tests are acceptable for both long and short term estimations of the friction angle and cohesion (Das & Sobhan, 2018). Where the cohesion is high, undrained tests are appropriate for short term and drained tests are used for long term estimations (Das & Sobhan, 2018). A shear box test under consolidated-drained condition was performed by Ozcan et al. (2013). This seems appropriate because Ozcan et al. (2013) stated that the specific tailings' cohesion is neglectable. Drained tests are most appropriate for soil with high permeability (Das & Sobhan, 2018).

Another option for soil inspection is the use of a Cone Penetration Test (CPT). This allows for in-situ testing where a 60° cone with a $10cm^2$ base is pushed into soil (Das & Sobhan, 2018). From this test the cone end resistance, and often the frictional resistance, is obtained (Das & Sobhan, 2018). Through calculation, the soil friction angle and vertical effective stress can also be obtained (Das & Sobhan, 2018). The CPT is less expensive than test requiring bores, but it does not allow for visual observations of the tested material (Das & Sobhan, 2018).

2.3 Foundation failure

Foundation failure occurs when the bearing capacity of the soil is overcome by the weight applied (Knight, 2015). This weight increase can be due to the building of the dam. If the soil is cohesive, the bearing capacity will increase over time, thus the rate of construction must be controlled (Knight, 2015).

2.4 Rate of rise

Another limiting factor to the life of a dam is the allowable deposition rate, also referred to as the Rate of Rise (Lebitsa, 2016). In South Africa the Rate of Rise for tailings dams is limited to 2 – 3m per year by the Chamber of Mines of South Africa (Lebitsa, 2016). This limitation has several justifications, one such is the ability to limit pore water pressure (Lebitsa, 2016).

2.5 Knowledge gap identified summary

The research on ash dams is sparse and heavily outweighed by work on tailing dams.

Tailing dam material, being waste from mining activities, has a much bigger grain size than fly-ash and will react differently in construction. Fly-ash undergoes cementation over long periods, thus it is also different from most clay material. The combination of these would make the rate-of-rise limitation used for tailing dams, conservative.

The research found mostly focuses on one or a combination of the following; slope stability, foundation stability and seepage. Other areas of research look at elements like rate of rise in isolation.

No examples of tailing dams or ash dams were found that do not have toe drains installed.

2.6 Conclusion

The failure mechanisms that accompany earth dams are; fall, topple, slide, flow bearing failure, internal erosion, surface erosion, hydraulic uplift or excessive soil deformation. Most commonly the factor of safety of a dam, which should be above 1.5, is assessed using limit equilibrium methods. Limit equilibrium methods assess sliding failures.

There are several limit equilibrium methods, and they include but are not limited to; Ordinary-, Bishop's simplified-, Method of slices for steady state seepage, Spencer's solution, Morgenstern's-, Morgenstern and Price- and Fellenius or Swedish- method.

The Ordinary method is conservative, does not account for pore water pressure, and is inaccurate for flat slopes. It performs best where angle of friction = 0.

In the Bishop method, forces on the sides of each slice is accounted for to some extent (small effect). It is used where a wide range of strata is present, but has a 2-7% inaccuracy. It does not account for pore water pressure. Sometimes numerical problems exist, and the FOS gained should be lower than that gained from the Ordinary method. It does not satisfy equilibrium with respect to forces, only moments.

The Steady state seepage method is a modification of Ordinary and Bishop methods.

The Spencer method uses stability charts.

Morgenstern can be used for rapid drawdown conditions. It is also a modification of the Bishop's method, and charts are available in this method.

The Morgenstern and Price method is the most accurate for dam embankments, because of the ability to assess rapid drawdown and circular and non-circular failure surfaces. The implied state of stress needs to be checked to ensure that no shear failure nor state of tension is implied. This is done by checking the shear force against the shear resistance of each slice. The line of thrust must lie above failure surface for solutions to be valid.

Fellenius' method is not recommended and has a 5-20% error.

Another way to assess the stability of an earth dam is through numerical methods. There are two major groups, continuum and discontinuum methods. In continuum methods everything is connected and discontinuum methods particles can dislodge and reconnect.

The continuum methods include; finite differencing method (FDM), finite element method (FEM), boundary element method (BEM) and finite volume method (FVM).

In FVM volume integrals in partial differential equations are converted to surface integrals using divergence theorem.

FEM is based on principle of virtual displacement. It uses matrix equations, and forces are applied at the nodes. It requires a complicated analysis but has the ability to evaluate nonlinear stress-strain behaviour. It can be used in continuous or quasi-continuous material. Pore-water pressure, movement, deformation, stresses within slopes, cracking and fractures can be evaluated. This method gives a high degree of realism. Hydraulic fracturing can also be assessed where the total normal stress is less than the local value of pore water pressure. It is however expensive and time consuming and requires specialized training with high-end computing resources.

In FDM differential equations are reduced to linear equations. It can model non-linear and dynamic problems, using field equations (Partial differentiation displacement vs time) and accounts for discontinuities. It also uses the friction laws (coulomb) to relate shear stress with normal stress. Displacement between grid points are used to determine the slip along discontinuity. It is a forward scheme and does not require iterations.

BEM is used in small boundary to volume ratio, where the continuum is static, elastic behaviour is present and stresses or displacement is applied to the boundary. It is not applicable where yielding occurs, gravity is significant or dynamic loading is present. It is normally used where the volume being analysed is large.

The discontinuum methods include the distinct element method (DEM), discontinuous deformation analysis (DDM) and the bonded particle method (BPM).

DEM can be used for 3D analysis. The domain is divided into blocks, interconnected through discontinuities, with the blocks being able to detach and reattach. It uses Newton's second law of motion. It requires large amounts of time to run and lot of storage, but it is nevertheless a very versatile method.

DDM can also be used for 3D analysis. DDM is an explicit method and its procedure resembles FEM. Springs are used to stop penetration or tension between elements. It relies on the equations of equilibrium.

In BPM, Finite difference algorithm is used to determine forces acting on a particle, which is used to solve Newton's second law of motion.

The limit state method is used to assess slopes that are on the verge of failure.

Artificial learning methods are not verifiable and should not be used.

3D methods give less conservative values in general, and are largely less subjective than 2D methods.

3 Methodology

The following activities were undertaken in this research:

1. A comprehensive literature review on the past research study conducted on stability analysis of Geotechnical structures using numerical tools,
2. Review of the background data and information on the dam including available geo-technical information and current slopes was done,
3. The geo-technical characteristics was decided on,
4. The stability of the ash dam using the Morgenstern and Price method, through Slope/W, and a numerical method, through FLAC3D, was done.
5. The deformation of the dam was assessed through FLAC3D
6. A sensitivity analysis was done using FLAC3D

3.1 Research instruments

In this research FLAC3D 7.00.122 as per the ITASCA Consulting Group, Inc and GeoStudio 2020 SLOPE/W 10.2.1.19666 was used to evaluate the stability of the slopes. SketchUp Pro 2019 version 19.3.253 64-bit was used to create the geography from the aerial surveys that was available in *.dwg format. This was run on a Dell Inspiron 3543 with an Intel® Core™ i7-5500U CPU @ 2.40GHZ and 8.00GB installed ram. The operating system used was Windows 10, version 1909.

3.2 Geotechnical investigation

The following steps were completed as part of the geotechnical investigation;

1. Old reports and other available information on the sub-soil conditions were analyzed.
2. Old reports and other available information on the ash characteristics were analyzed.
3. Visual inspections around the site was done. The invasive trees on the embankment opposite the dam was removed to assess the soil distribution around the dam and for environmental considerations. The color of the soils was compared to the soils reported in the geotechnical evaluation.

3.3 Geology around Arnot's Ash Dam

3.3.1 Ash on the dam

The coal ash will greatly depend on the properties of the coal being used. At Arnot, coal is received from various sources and these sources have changed during the life of the station. It is therefore difficult to find ash specimen that will represent the whole of the dam. The literature is therefore also reviewed to obtain values along with on-site evaluations.

About 87% of the ash produced at a power station is fly ash, the remaining 13% is coarse ash (Zielke-Olivier & Vermeulen, 2019).

3.3.2 Geotechnical evaluation done in 1990

A geotechnical evaluation was completed in 1990 around the circumference of the dam as seen in the following figure 24.

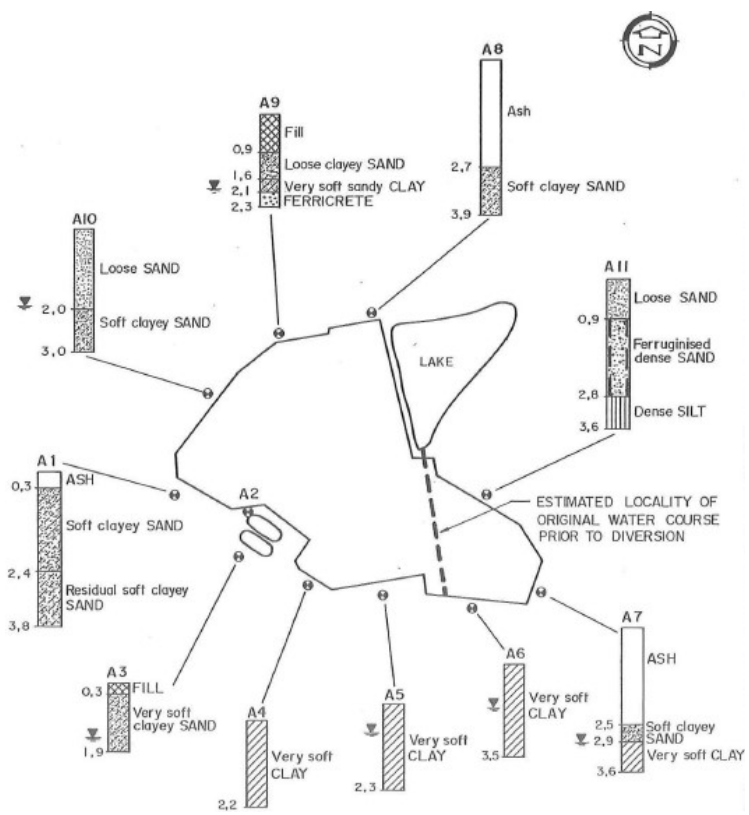

Figure 24 Geotechnical evaluation completed in 1990 (Brackley & Erwin, 1990)

This evaluation was not done around the then unconstructed Flamingo pan ash dam. It also does not show the extent to which any of the material extends underneath the dam, and requires assumptions in this regard but, during a maintenance activity of the spring/ tributary diversion, done as part of this research, the material was inspected, which was compared to the map in figure 24 and colours in table 3, and added more detail to the eastern side of the impoundment was obtained. The exact position of the surface Grey-black clay was identified. A summary of the original test results is given in the table below:

Table 1 Laboratory lab results summary – soil types (Brackley & Erwin, 1990)

Test Pit	Sample	Description	Depth (m)	Moisture Content (%)	PI	Clay %
TP A1	A2	Clayey Sand	3,4	37	20	7
TP A3	A2	Clay	1,5	20	14	26
TP A4	UDA 3	Clay	1,8	44	45	36
TP A5	UDA 4	Clay	1,7	24	29	30
TP A6	A5	Clay	1,0	35	36	35
TP A8	UDA 6	Ash	1,0	-	-	3
TP A8	A7	Clayey sand	3,3	18	9	11
TP A9	A8	Sandy clay	1,8	28	9	12
TP A10	A9	Clayey sand	2,5	23	9	7

Table 2 Laboratory test results - Strength and coefficients of consolidation (Brackley & Erwin, 1990)

Test-Pit	Sample	Descrip-tion	Depth (m)	Effective Strength		Cv (m^2/yr)
				c'	ϕ'	
TPA 4	UDA 3	Clay	1,8	0	15	0,15
TPA 5	UDA 4	Clay	1,7	-	-	0,17
TPA 7	UDA 5	Ash	1,0	10	38	-

3.3.3 Calculating the Shear and Bulk Modulus

FLAC3D requires the Shear and Bulk Modulus, or Young's modulus and Poisson's Ratio as inputs. The shear strength is a function of frictional resistance between particles, cohesion and moisture content (Das, 2005). The shear stress is approximated as a linear function of normal stress, and the relationship is as follow by Das (2005):

$$\tau_f = c' + \sigma' \, tan\emptyset'$$

Where

c' = effective stress cohesion

$\emptyset'$ = effective angle of internal friction

σ' = effective stress on the failure plane

τ_f = shear stress on the failure plane

The effective stress cohesion (c') for sand and inorganic silt is 0 (Das, 2005). For consolidated clays it can be approximated at 0 and for over-consolidated clays c' is greater than 0 (Das, 2005).

Table 3 Material around the ash dam (Brackley & Erwin, 1990)

Material	Location	Wet Density (kg/m^3)	Effective Cohesion (kPa)	Effective Friction Angle
Grey-black clay	Vlei, South side	2 000	0	15
Orange-brown clayey sand and sandy clay	Remainder of perimeter	2 000	5	30
Ash	In dam	1 500	0	34

3.3.3.1 For the Grey-black material:

Poisson's ratio (v) is estimated as $= \frac{1-sin\,\emptyset}{2-sin\,\emptyset} = \frac{1-si\quad 15}{2-sin\,15} = 0.43$

Young's modulus (E) = Stress/strain = 45/2 = 22.5

Bulk modulus (K) $= \frac{E}{3(1-2v)}$

Shear modulus (G) $= \frac{E}{2(1+v)}$

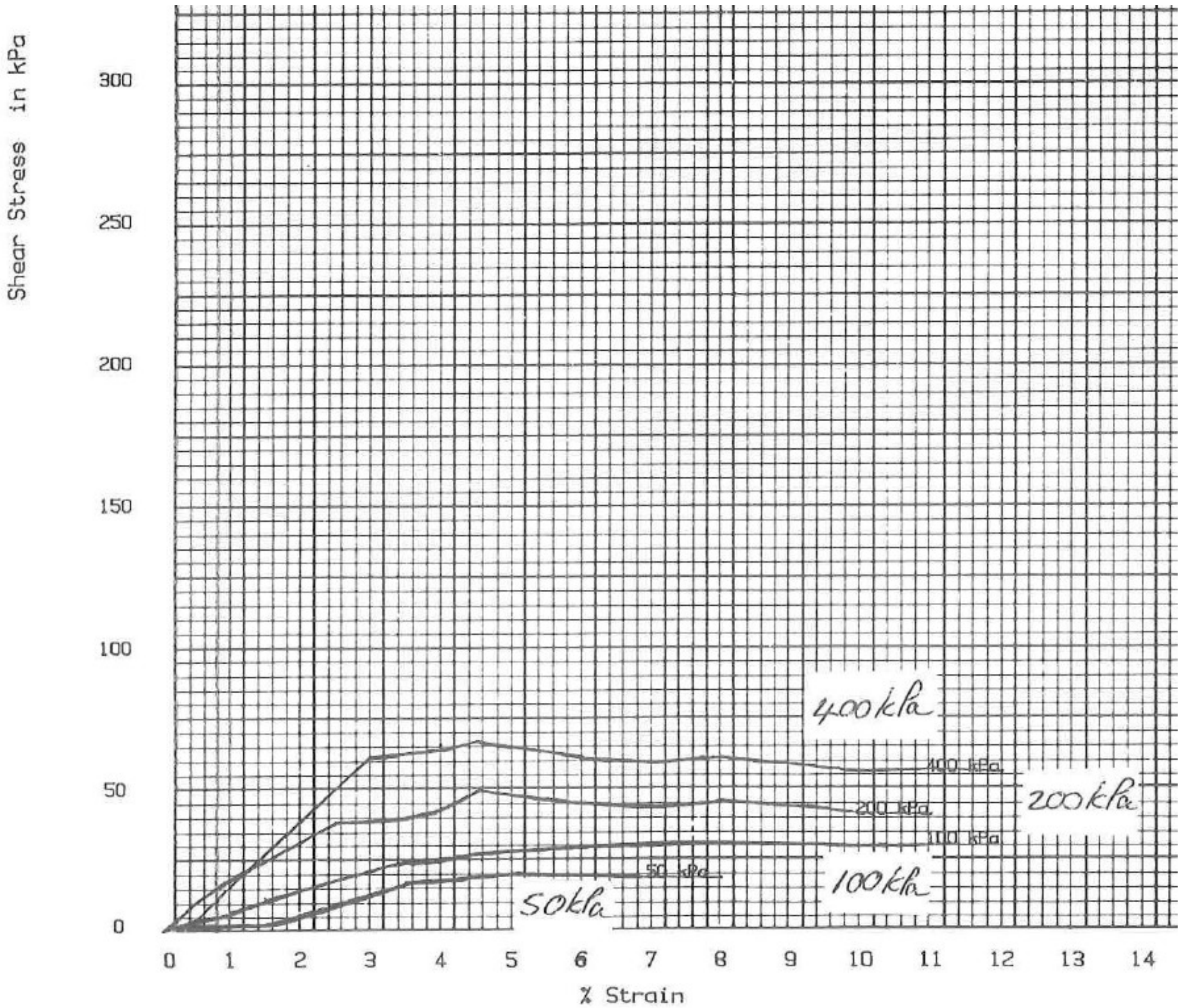

Figure 25 Stress and strain diagram for Grey-black material (Brackley & Erwin, 1990)

3.3.3.2 For ash

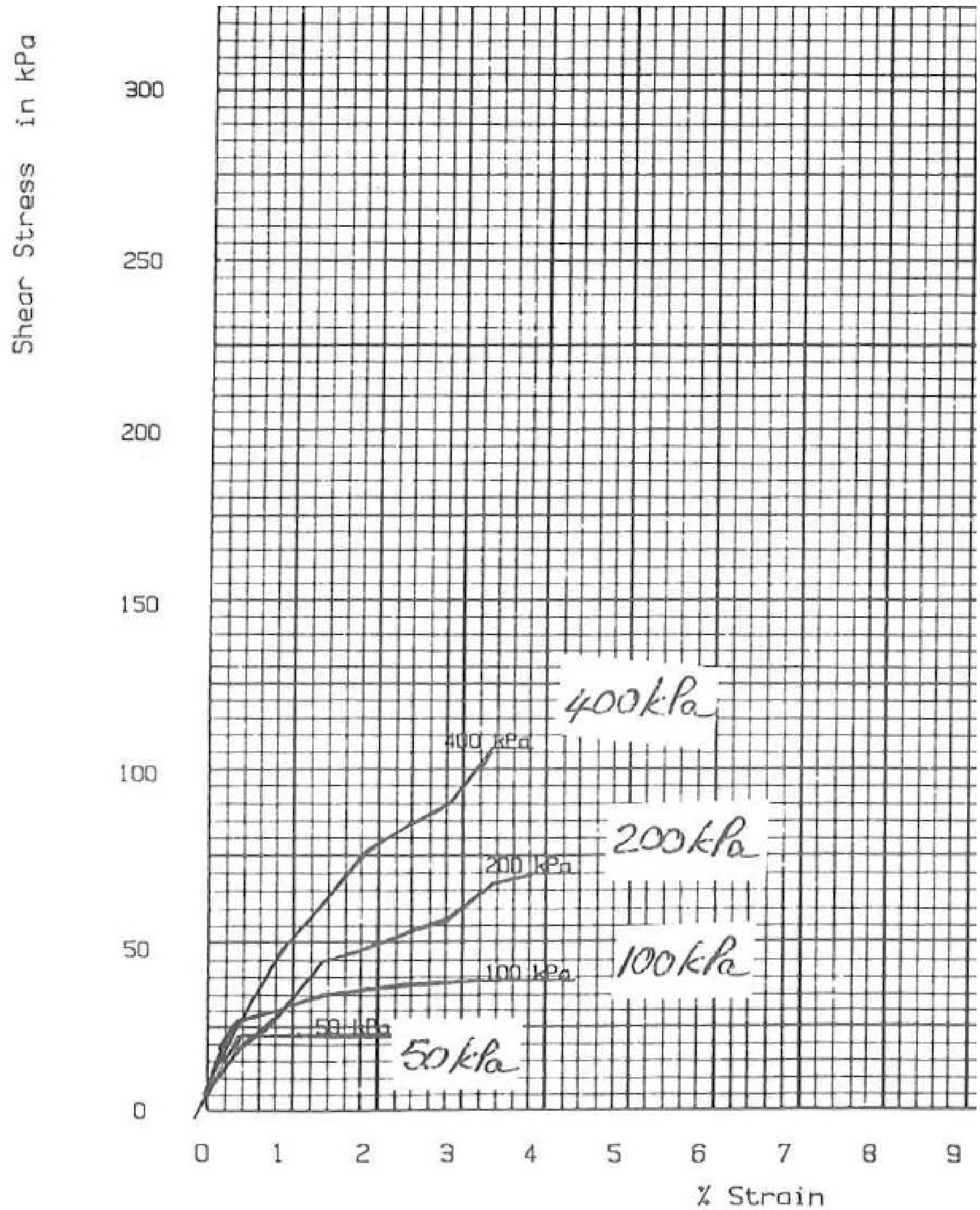

Figure 26 Stress and strain diagram for ash (Brackley & Erwin, 1990)

Young's modulus (E) = Stress/strain = 50/1 = 50

Poisson's ratio is estimated as $= \frac{1-sin\,\emptyset}{2-sin\,\emptyset} = \frac{1-sin\,34}{2-sin\,34} = 0.31$

Bulk modulus (K) $= \frac{E}{3(1-2v)}$

Shear modulus (G) $= \frac{E}{2(1+v)}$

3.3.4 DCPs and geotechnical analysis done in December 2019

3.3.4.1 DCP test results

Eight DCP tests were conducted on the ash dam by Golder Engineering (Lekgau, Mazibuko, & Marais, 2019). These tests results are presented in figure 27 below:

Figure 27 DCP locations (Lekgau et al., 2019)

Table 4 DCP test results (Lekgau et al., 2019)

<table>
<tr><th rowspan="3">Ash Dam Location</th><th rowspan="3">DCP No.</th><th rowspan="3">Total depth (m)</th><th colspan="4">Interpretive Consistency at depths (m) – (m)</th></tr>
<tr><th colspan="4">Cohesive Soils</th></tr>
<tr><th>Soft</th><th>Firm</th><th>Stiff</th><th>Very Stiff to Near Refusal</th></tr>
<tr><td rowspan="5">Beach</td><td>DCP1</td><td>3,0+</td><td>-</td><td>0 – 0,3</td><td>2,7 – 3,0+</td><td>0,3 – 2,7</td></tr>
<tr><td>DCP2</td><td>3,0+</td><td>-</td><td>0 – 0,2</td><td>0,2 – 1,8</td><td>1,8 – 3,0+</td></tr>
<tr><td>DCP3</td><td>3,0+</td><td>0 – 0,6</td><td colspan="2">0,7 – 1,5</td><td>0,6 – 0,7
0,7 – 3,0+</td></tr>
<tr><td>DCP4</td><td>3,0+</td><td colspan="2">0,9 – 1,7</td><td>0 – 0,9</td><td>0,9 – 3,0+</td></tr>
<tr><td>DCP5</td><td>3,0+</td><td>0 – 0,2</td><td colspan="2">0,3 – 1,6
2,4 – 2,9</td><td>0,2 – 0,3
1,6 – 2,4
2,9 – 3,0+</td></tr>
<tr><td rowspan="3">Bench</td><td>DCP6</td><td>0,73+R</td><td>-</td><td>0 – 0,6</td><td>-</td><td>0,6 – 0,73+R</td></tr>
<tr><td>DCP7</td><td>0,73+R</td><td>-</td><td>-</td><td>0 – 0,1</td><td>0,1 – 0,73+R</td></tr>
<tr><td>DCP8</td><td>2,8+</td><td>-</td><td>-</td><td>0,6 – 1,1
1,4 – 2,8+</td><td>0 – 0,6
1,1 – 1,4</td></tr>
</table>

Table 5 DCP interpretation (Lekgau et al., 2019)

Description	DCP (mm per blow)	Bearing Capacity kPa
	Cohesive Soils	
Very Soft	>110	<35
Soft	55 -110	35 - 75
Firm	30 - 55	75 - 150
Stiff	15 - 30	150 - 300
Very Stiff	5 - 15	>300

All the DCP test were done along the route of a new proposed penstock line. DCP 1 to 5 were all done in the pool area where coarse ash is prevalent, but fly-ash was deposited there to provide a platform for the construction of this line. This will explain the 3m thick top layer of stiff to very stiff material. Of note is the early refusals of DCP6 and DCP7, which is located on the fly ash zones. These refusals are unlikely because of stones or other foreign material and a more probable cause is the cementing action of fly ash, which is very possible when taking the age of the material into consideration. Another possibility reported by Golder for the refusal, is the high moisture content in the ash material. A high phreatic surface can be seen in the area when the piezometers are evaluated.

3.3.4.2 Laboratory test results on ash samples

Five ash samples were taken at DCP1, DCP3, DCP6 and DCP7. These were analysed by Soillab in Pretoria. The following tests were done:

- Foundation indicator tests were done on all samples (Grading, Atterberg limits and Hydrometer)
- Standard proctor compaction tests were done on 3 samples
- Natural moisture content was evaluated on 3 samples
- Shear box tests on recompacted ash samples, recompacted to 95% standard proctor density at optimum moisture content conducted at 150kPa, 300kPa and 600kPa.

Table 6 Summary of laboratory test results on ash samples (Lekgau et al., 2019)

SAMPLES		GRADING (%)				ATTERBERG LIMITS (%)			MOISTURE CONTENT (%)	GM	PE	USC	STANDARD PROCTOR COMPACTION		SHEAR BOX		DESCRIPTION
No.	*Depth (m)	Gravel	Sand	Silt	Clay	LL	PI	LS					MDD (kg/m³)	OMC (%)	COHESION (kPa)	ANGLE OF INTERNAL FRICTION (°)	
DCP1/1	0-0.3	0	43	44	13	-	NP	0	50	0,3	Low	ML	1060	16	11	32	Ash
DCP3/1	0-0.3	0	29	46	25	-	NP	0	-	0	Low	ML	-	-	-	-	Ash
DCP5/1	0-0.3	0	34	48	18	-	NP	0	31	0,1	Low	ML	1084	15	9	33	Ash
DCP6/1	0-0.3	0	49	38	13	-	NP	0	28	0,3	Low	ML	1109	15	2	34	Ash
DCP7/1	0-0.3	2	56	33	9	-	NP	0	-	0,6	Low	ML	-	-	-	-	Ash

Because the shear box tests were remoulded the effect of cementation is not seen. These values are similar to the 1990 values for the fly-ash and validates those results.

3.3.5 Visual inspections

The spring diversion was overgrown with invasive trees. The trees on the embankment of the river that is not on the side of the ash dam was removed to make the embankment slopes clear. The soil was inspected, to enable the visual identification of various types, and compared to the 1990 geotechnical report in which the colors were noted. The trees on the side of the dam is left alone, because of their assumed structural significance to the slope.

3.4 Determining the geographical properties of the dam and developing models

Two methods were used to create the FLAC3D models. The one was using the standard extrusion method explained in Itasca Consulting Group (2017a). This method is not explained here. The second method is by using SketchUp.

An aerial survey, which was available from before this research, with 0.5m contours, that was conducted using Airborne Laser Scanning and Digital Imagery Data from a fixed wing aircraft, was used to create the geometries needed for the models. This aerial survey of the ash dam, which was drawn in DXF format, was imported into Google Sketchup, shown in figure 28. The drawing's scale was easily updated by using the known height difference between contour lines and Sketchup's tape measure tool. When the measuring tool is used, one would left click on a contour, press the upwards key, and click on the contour directly above or below. Without clicking again, 0.5m is typed and enter is pressed. This would scale the drawing.

One of the strengths of 3D analysis is that irregular shapes can be evaluated. For this reason, the area that was selected had the most irregular shape.

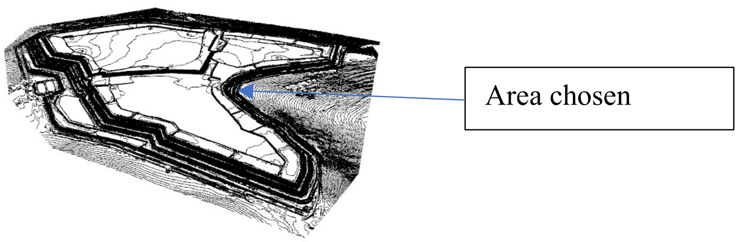

Figure 28 Aerial survey imported into Sketchup

ITASCA recommends that a critical area be chosen for analysis to reduce the time required for calculation. The area that was chosen is where Flamingo Pan and Ash dam 2 meets, because of the interesting geometry and it includes the spring/ tributary diversion, the location is shown on figure 29. The area of contours needed was selected as shown in figure 29 and transferred to a clean SketchUp window.

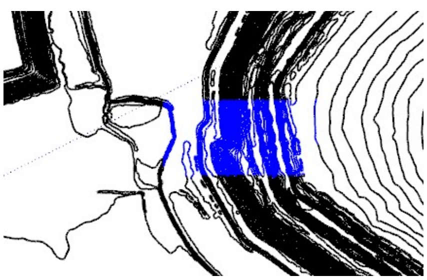

Figure 29 Selecting of contours in Sketchup

The Group function in SketchUp is used to group the contours that correspond with ash and the contours that are part of the foundation material. An old drawing, figure 30, of the contours of the area before the dam was constructed was used to populate additional contours under the dam that was grouped with the foundation material. The alignment was then changed to be perpendicular with the axis in SketchUp.

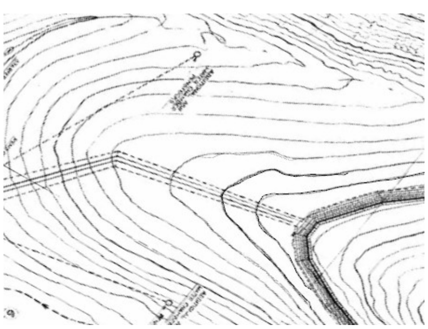

Figure 30 Foundation contours of ash dam

3.4.1 Creating models for FLAC3D

After the two groups were created in Sketchup, the "Sandbox from contour" tool was used to create two surfaces, one for the ash and one for the underlying foundation material, as shown in figure 31 - 33.

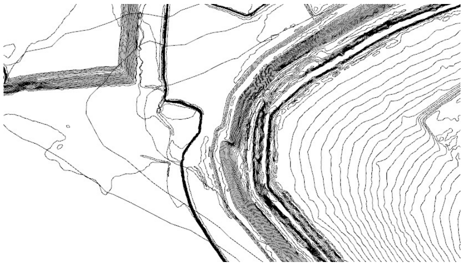

Figure 31 Meshing of contours in SketchUp

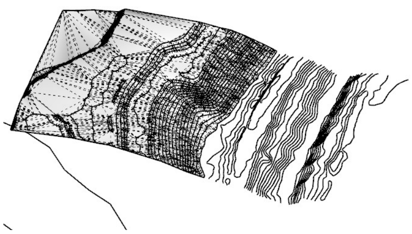

Figure 32 Creating skin for ash material

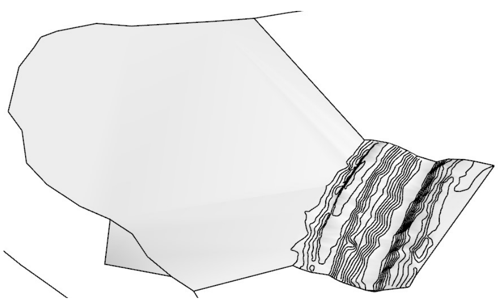

Figure 33 Creating a skin for the underlying material

Sketchup allows files to be exported as *.stl, which in turn can be imported by FLAC3D. The surface is imported directly into the building blocks tab of FLAC3D. A building block is then created and sized smaller than the surface. Figure 34 and 35 shows the imported "skin" and 36 the building block.

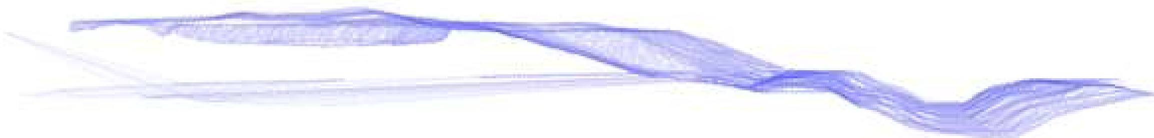

Figure 34 Surface imported into FLAC3D

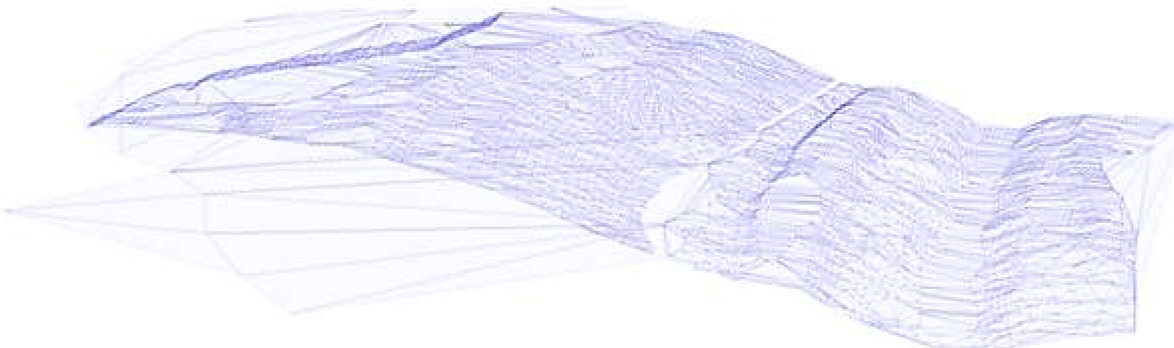

Figure 35 Surface imported into FLAC3D

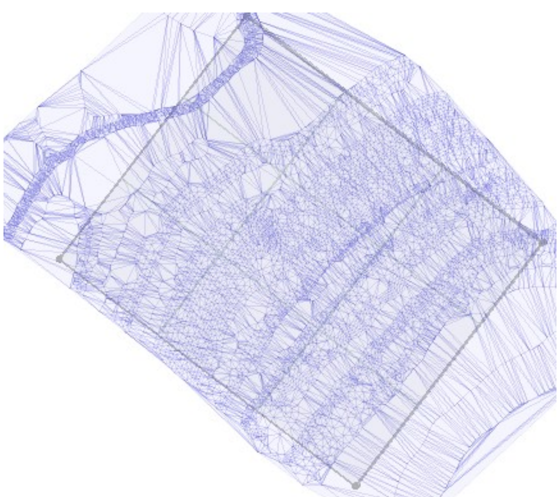

Figure 36 Sizing of building block

The building block is split in areas of high geometrical detail as shown in figure 37.

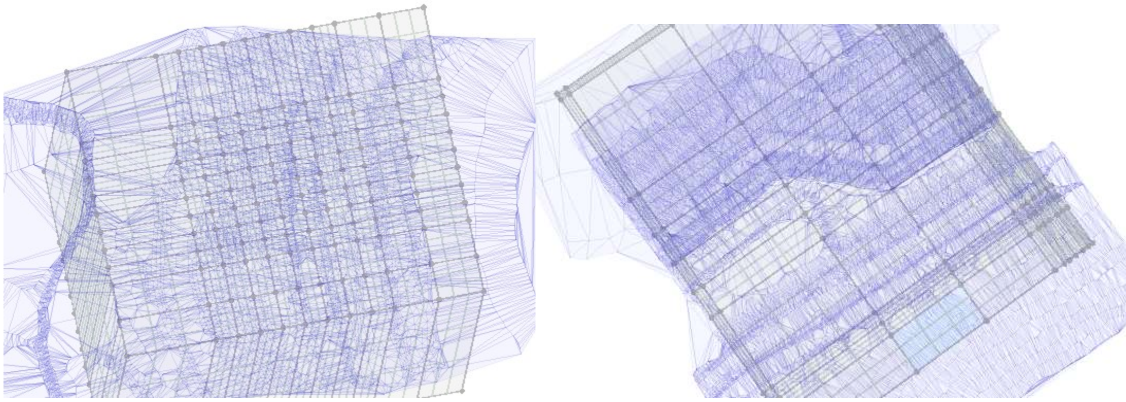

Figure 37 Splitting of blocks

The split blocks are then draped downwards onto the surface, using the drape function under object properties in the building block tab, as shown in figure 38 and 39. The "skin" is hidden temporarily to see how well the building blocks represents the skin, as shown in figure 40. More blocks can be split if it does not represent the geometry correctly, and the draping tool reused.

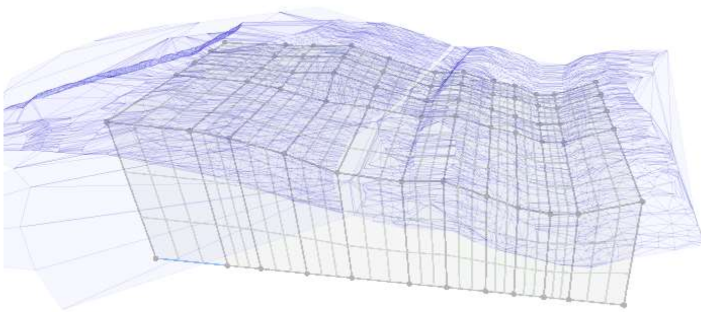

Figure 38 Draping of block onto surface

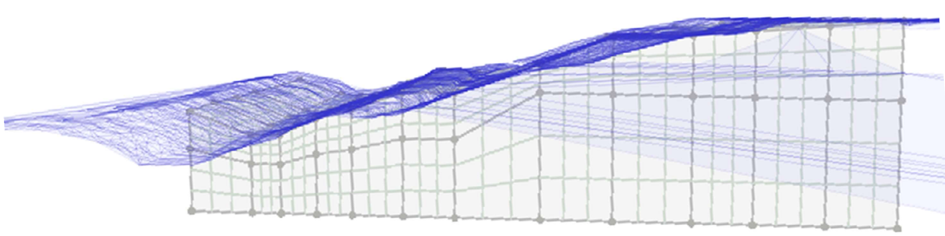

Figure 39 Draping of blocks side view

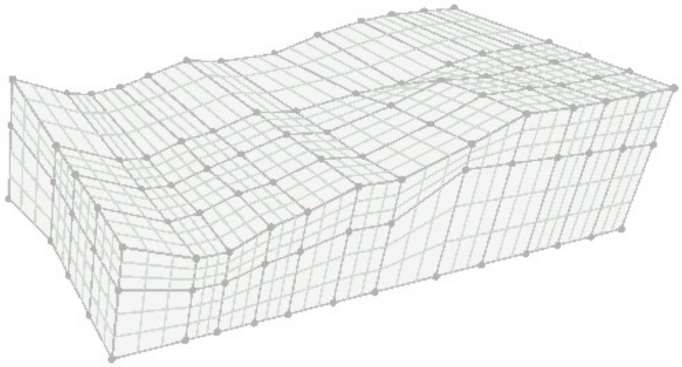

Figure 40 Removal of geometry from building blocks

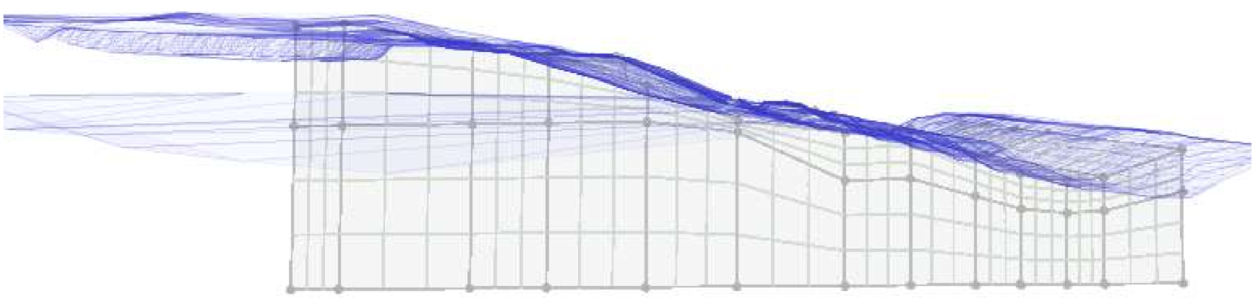

Figure 41 Draping of second layer onto underlying material

The building blocks are also split in the horizontal plane as shown in figure 41. This allows the second layer to be draped onto the foundation material.

Zones are then created in the model tab and the area with fly ash was selected and a name assigned “ash”. This is shown in figure 42.

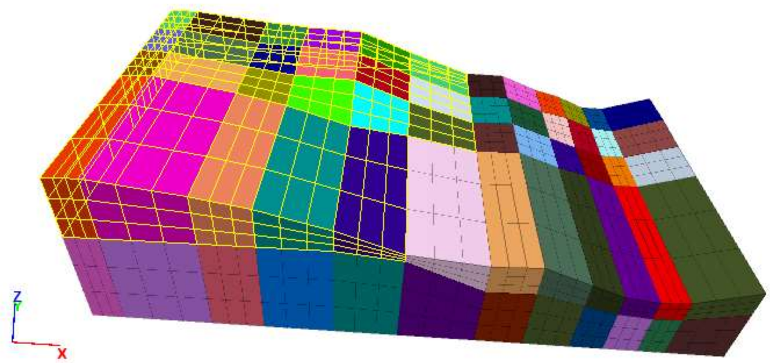

Figure 42 Creating groups in model

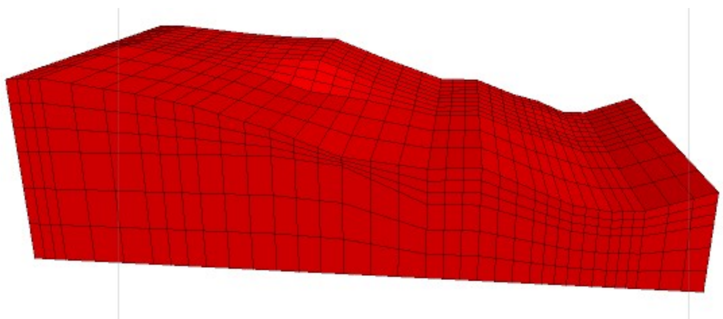

Figure 43 Model presented in the plot tab

3.4.2 Creating a corresponding 2D model to be used in Slope/W

Using the imported contours from the creation of the FLAC3D model, a face/ plane is created in Sketchup where the weakest section is chosen/guessed, as shown in figure 44 and 45. The contours are removed as shown in figure 46 and redrawn as per 47. Dimensions are added as per figure 48 and this is redrawn in Slope/W.

Slope/W was used to apply the Morgenstern and Price Method to evaluate a profile of the impoundment and where the spring/ tributary diversion also occurs. By using the information gained from the piezometers and the water level inside the river, it was seen that the phreatic surface was close to the surface and the geotechnical information only had saturated values. For this reason, the phreatic line was not added. Because there exists uncertainty of the extent of the very soft grey-black material, the foundation was also modelled using this.

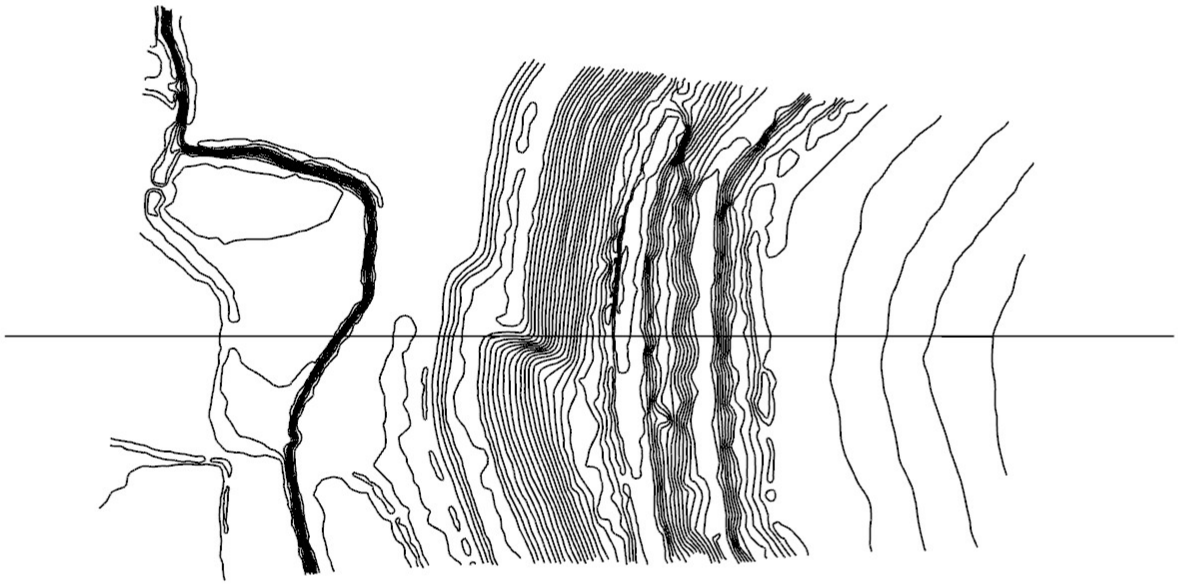

Figure 44 Creating a face at the weakest section

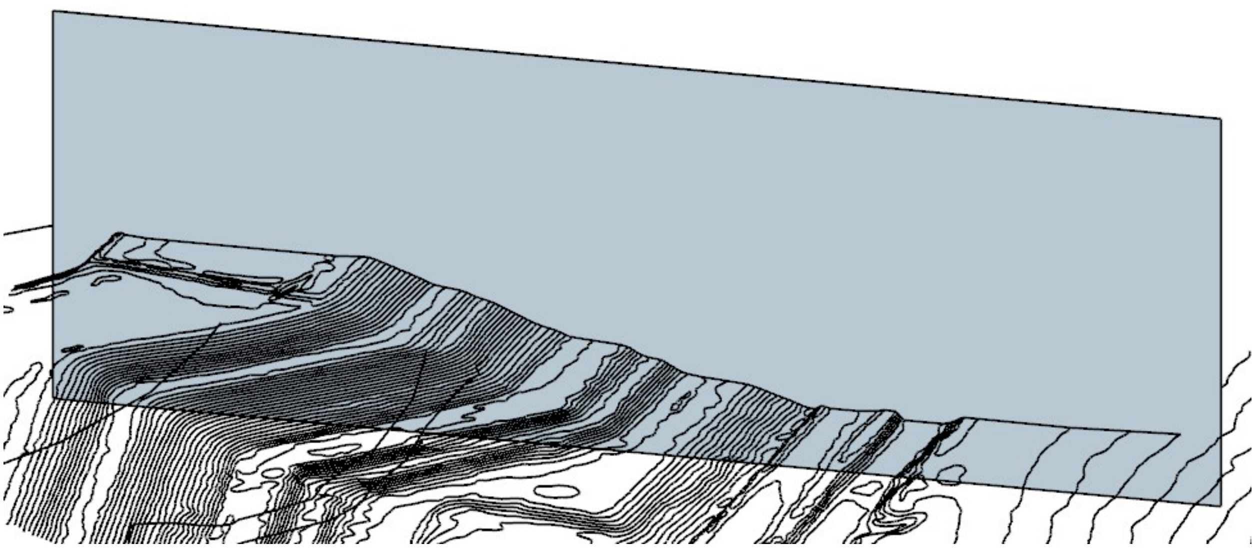

Figure 45 Creating a plane on slope

Figure 46 Connecting the contours to gain a section

Figure 47 Simplified section to be used in Slope/W

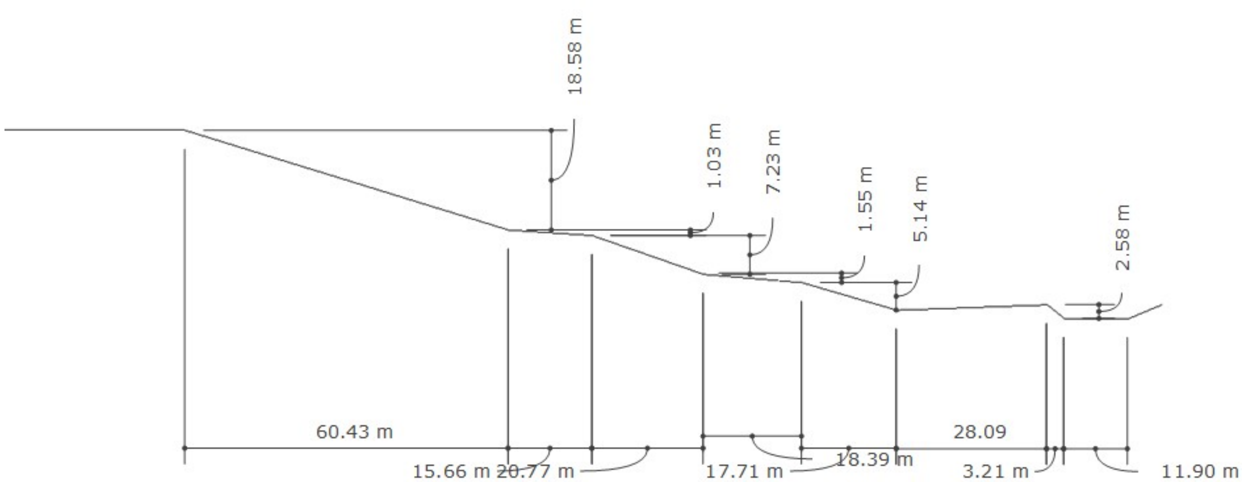

Figure 48 Dimensions of simplified section to be used in Slope/W

3.5 Evaluate the stability of the ash dam using numerical modelling software and limited equilibrium methods.

FLAC3D and Slope/W was used to estimate the factor of safety for the slope. Because the walls of the dam are constructed from fly ash, the walls will be taken as consisting of a monolithic material, not taking into account the underlying material. This will enable this program to be used with circular slips. No distinction is made for different types of fly-ash because the sources cannot be traced. Cementing action in the fly ash is also not considered.

A sensitivity analysis is done by changing the geotechnical parameters one by one, in FLAC3D. The foundation material is also alternated between the Orange-brown material and Grey-black material, to gain a limited understanding of the combined effect of changing more than one parameter at a time.

3.6 Example if code used in FLAC3D for analysis

This example is for where the foundation material is the Grey-black material.

```
zone face skin

; Constitutive model and properties

zone cmodel assign mohr-coulomb

zone property density 1500 young 50 poisson 0.31 cohesion 1000 ...

friction 34 range group "ash"

zone property density 2000 young 22.5 poisson 0.43 cohesion 0 ...

friction 15 range group "ash" not

; Boundary conditions

zone face apply velocity-normal 0 range group 'East' or 'West'

zone face apply velocity-normal 0 range group 'North' or 'South'

zone face apply velocity (0,0,0) range group 'Bottom'

; Initial conditions

model gravity 9.81

zone initialize-stresses

model largestrain false

; Histories

model history name='conv' mechanical convergence

; Solve

model solve convergence 1
```

```
model factor-of-safety file 'Grey-blackFOS01' associated convergence 1
```

The “unstable” results are used, and the displacement is plotted, as this represents the failure surface as per the FLAC3D 6.0 example manual.

3.6.1 Initializing of the model

Each time a model is run, there is residual loads left from the previous analysis. This is to enable one to track changes of material in situations like excavations. For this reason, the model needs to be initialized each time new parameters are used in the sensitivity analysis. FLAC3D, allows for the following commands to remove this history:

```
zone gridpoint initialize displacement (0,0,0)
zone gridpoint initialize velocity (0,0,0)
zone initialize stress
```

In this research, these were not used, instead the initial model was selected each time as a base to start the analysis. This ensured that no residual stresses, displacements, velocities or loads were overlooked.

3.7 Limitations

Arnot power station has historically received coal from a variety of mines. The resulting ash cannot be accurately mapped on the dam and the ash qualities must be approximated and is based on the results from the 1990 investigations.

The crystal formation of the ash is not investigated, only the results from geotechnical evaluations is.

The study does not include an investigation on the possible pollution of the ground water. This is monitored separately by the station.

The rate of rise of this ash dam is not studied.

Seepage through dam walls lead to piping. Because of the cementing properties of fly-ash, piping is less probable than on other dams. This said, piping on ash dams will not be assessed.

South Africa is not close to any fault lines, and liquification is not assessed.

The phreatic surface is very close to the surface of the wall’s side slopes. Geo-technical information is also only available for saturated soils. Pore-water pressure is not assessed.

The sensitivity of FLAC3D to the addition of more zones or increasing the geographical dimensions is not assessed.

3.8 Conclusion of the method statement

Historic geotechnical information was used to determine the soil parameters in the area. The river running in the area of analysis was stripped of trees on the embankment opposite the dam. This was visually inspected to determine the upper layers of the soil distribution.

The geotechnical parameters, along with an available aerial survey was used as inputs for the evaluation. Models were first created in SketchUp to make sure the models were consistent for FLAC3D and Slope/w.

4 Slope stability using the limit equilibrium method

The section chosen was analysed using Slope/W. The material properties used for this analysis reflects the material properties reported in the 1990 geotechnical evaluation. The foundation material was taken as the Orange-brown material and Grey-black material respectively. Because no record exists to show the type of material underneath the dam, the Grey-black and Orange-brown material is thus taken to be uniform underneath the dam.

The embankment that is on the opposite side of the ash dam is also evaluated.

A Half-Sine function was chosen and deemed appropriate because the slip circle did not pass through more than one material. Because the Morgenstern-Price method is deemed the most accurate, it was chosen for the analysis.

The tolerance of the factor of safety was put as 0.01, minimum slip surface depth as 0.1m, with 100 slices and the iterations as 100.

4.1 Slope stability in the area of the spring diversion with Orange-brown material foundation material

The material parameters chosen was as follow:

Ash:

Internal angle of friction = 34°
Cohesion = 0 kPa
Unit weight = $1500 kg/m^3 \times 9.81 \div 1000 = 14.72 kN/m^3$

Orange-brown material:

Internal angle of friction = 30°
Cohesion = 5 kPa
Unit weight = $2000 kg/m^3 \times 9.81 \div 1000 = 19.62 kN/m^3$

When the slip entry is defined as anywhere on the embankment the failure occurs in the Orange-brown material zone with a factor of safety of 1.907 and is shown in figure 49 and 50.

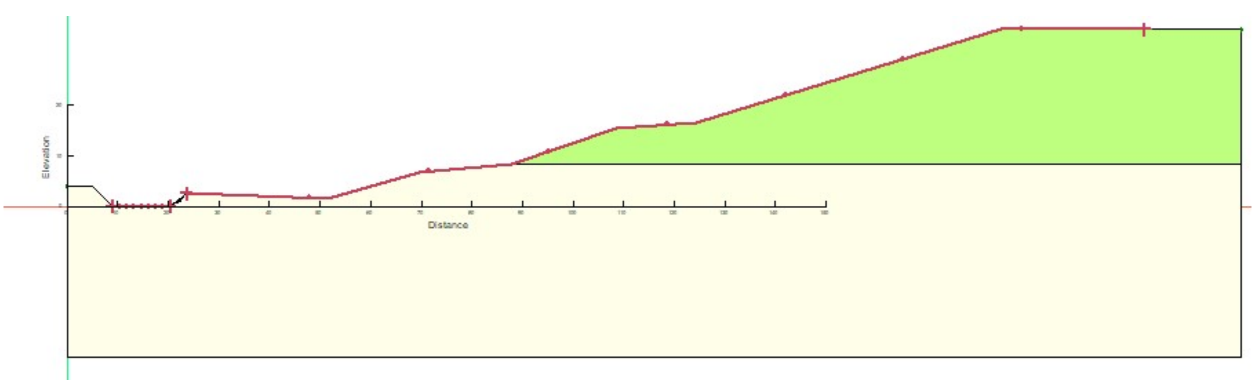

Figure 49 Overall slope stability in Orange-brown material – FOS = 1.907

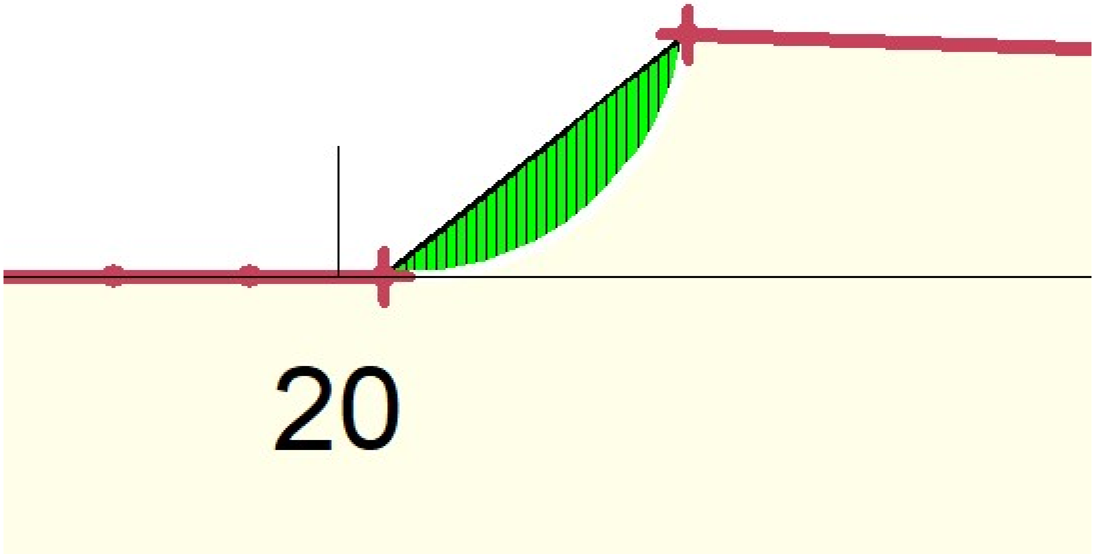

Figure 50 Closer view of failure in Orange-brown material material slope – FOS = 1.907

4.2 Slope stability in the area of the spring diversion with Grey-black

The material parameters chosen was as follows:

Ash:

Internal angle of friction = 34°
Cohesion = 0 kPa
Unit weight = $1500 kg/m^3 \times 9.81 \div 1000 = 14.72 kN/m^3$

Grey-black material:

Internal angle of friction = 15°
Cohesion = 0 kPa
Unit weight = $2000 kg/m^3 \times 9.81 \div 1000 = 19.62 kN/m^3$

When the slip entry is defined as anywhere on the embankment the failure occurs in the Grey-black material zone with a factor of safety of 0.336 and is shown in figure 51 and 52.

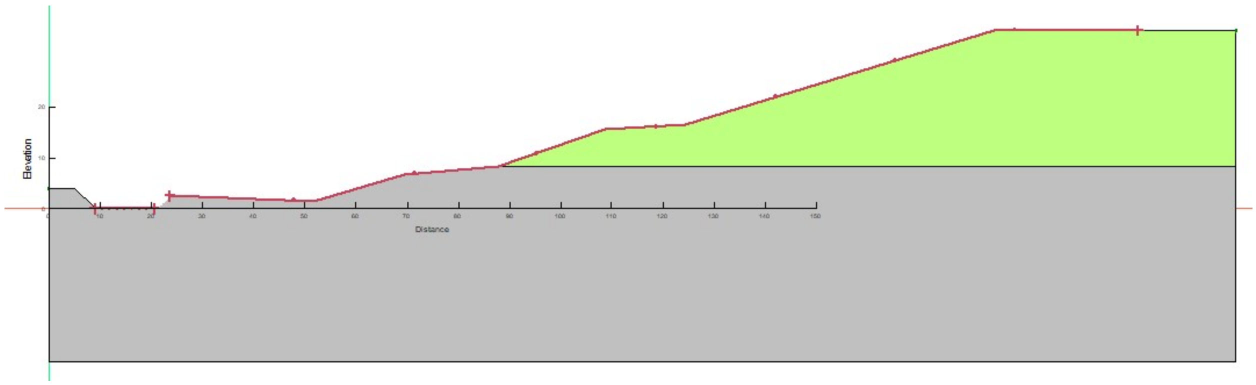

Figure 51 Overall slope stability in Grey-black material – FOS = 0.336

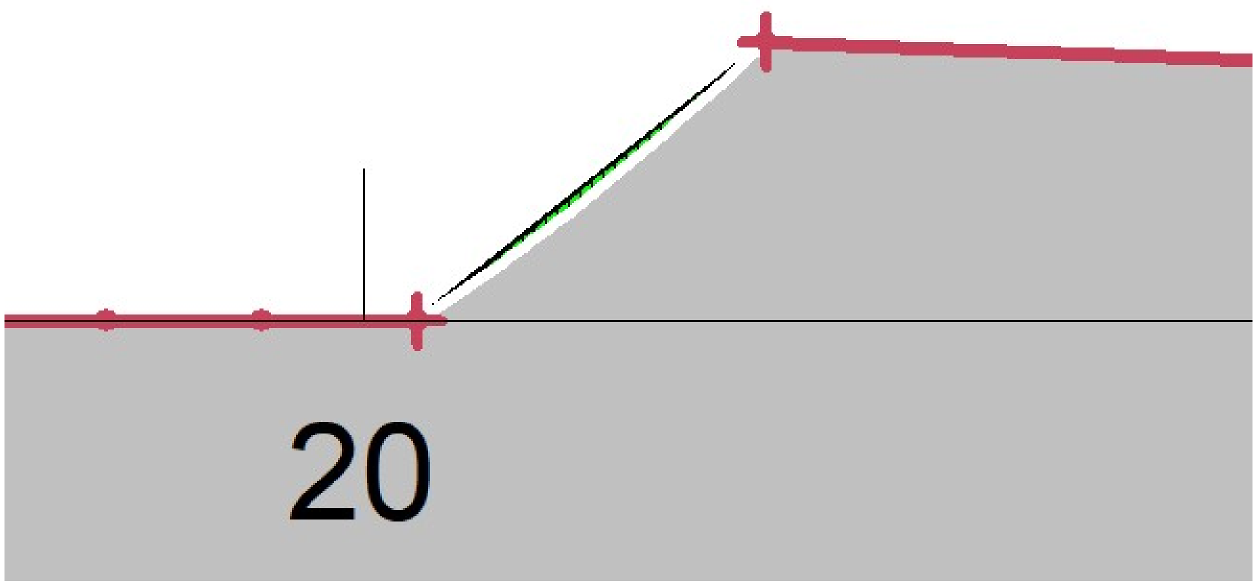

Figure 52 Closer view of failure in Grey-black material slope – FOS = 0.336

4.3 Slope for the spring diversion with Orange-brown material

The original design for the spring diversion had a 45-degree slope, as shown in figure 5, and has failed in several places as seen in figure 6. A section was used that was 9.45m high, and a factor of safety of 0.999 was obtained using the Morgenstern-Price method is Slope/W.

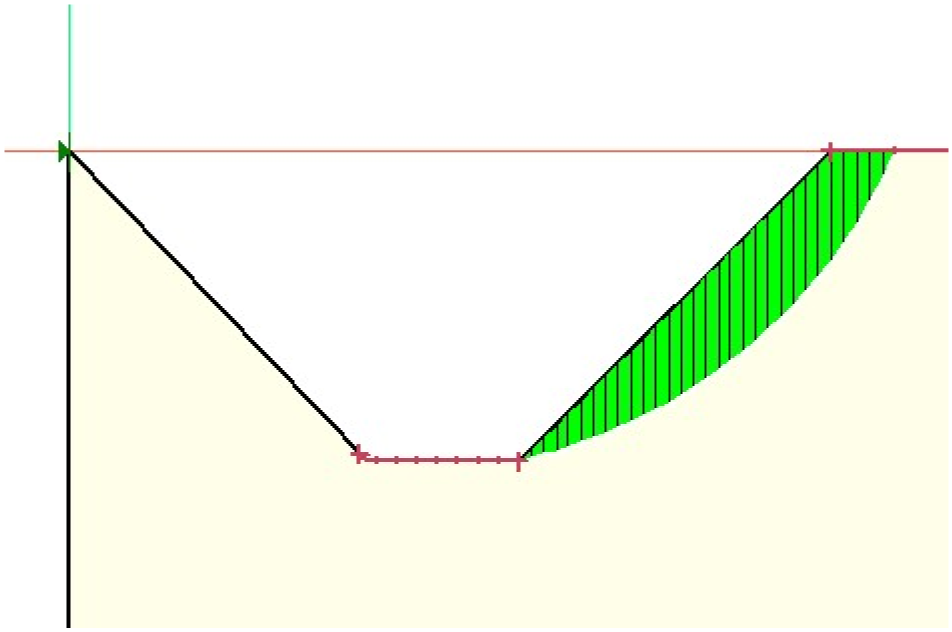

Figure 53 A 1:1 Slope with FOS of 0.999

Since the factor of safety is already so low when evaluating the previous slope using Grey-black material, the need to re-evaluate this slope using this higher angle is not deemed to be necessary.

5 Numerical analysis using FLAC3D

The Mohr-Coulomb method was used, as it is the recommended method by Itasca Consulting Group (2017a) for material that is loose or cemented granular materials, soils, and rock used in slope stability analysis.

The material in the area is mostly the Orange-brown material, with Grey-black material in some isolated areas. The values used are those obtained from the 1990 geotechnical evaluation, and a one-by-one sensitivity analysis was performed on these. The base values are given as follow:

Table 7 Material parameters used as base

	Cohesion (kPa)	Internal angle of Friction	Density	Poisson's Ration	Young's Modulus
Ash	0	34	1500	0.31	50
Grey-black	0	15	2000	0.43	22.5
Orange-brown material	5	30	2000	Not given in 1990 evaluation Taken as 0.2	Not given in 1990 evaluation Taken as 100

Some typical values for the Poisson's Ratio and Elastic Modulus (Young's Modulus) is given by Das (2011). For Orange-brown material a Poisson's Ration is given as between 0.15 and 0.25 and is assumed to be 0.2 for the Grey-black material. No material has a value of below 0.15 or above 0.5.

Typical values for the Elastic Modulus vary between 0.5 and 200, and sandy clay has values of between 25 and 200. A value of 100 is chosen for the Orange-brown material as base for this analysis.

5.1 Orange-brown foundation material for area 1

Where the Orange-brown material was used, the failure would happen in the ash region, as shown in figure 54, and would have a value of 1.988.

Table 8 Factor of Safety using FLAC3D for the Orange-brown foundation material

Factor of Safety of 1.988					
	Cohesion (kPa)	Internal angle of Friction	Density	Poisson's Ration	Young's Modulus
Ash	0	34	1500	0.31	50
Orange-brown material	5	30	2000	0.2	100

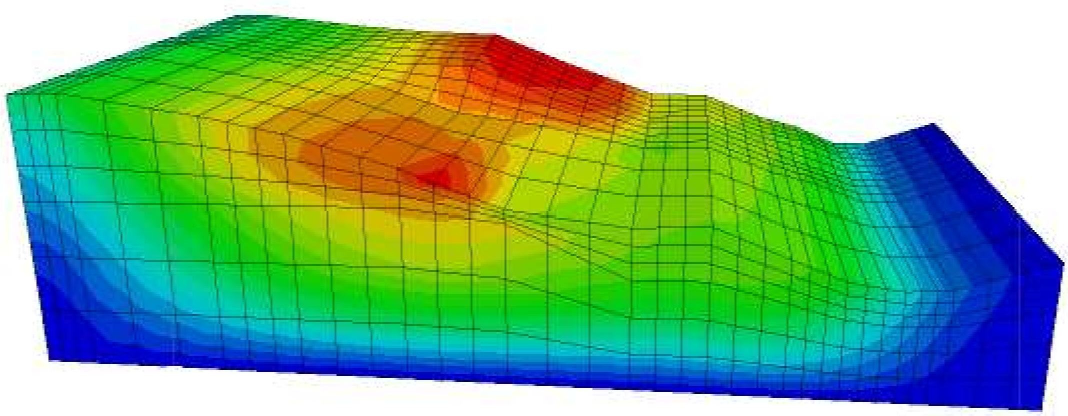

Figure 54 Failure in the ash region with a factor of safety of 1.998

5.2 Very Weak Grey-black foundation material for area 1

Where the foundation material is selected as being the Grey-black material, the foundation failed in the foundation region, as shown in figure 55 and has a factor of safety of 0.846. This is higher than the factor of 0.336 gained from the Limit Equilibrium analysis, but both show failures in the same zone.

Table 9 - Factor of Safety using FLAC3D for the Grey-black foundation

Factor of Safety of 0.846					
	Cohesion (kPa)	Internal angle of Friction	Density	Poisson's Ration	Young's Modulus
Ash	0	34	1500	0.31	50
Grey-black	0	15	2000	0.43	22.5

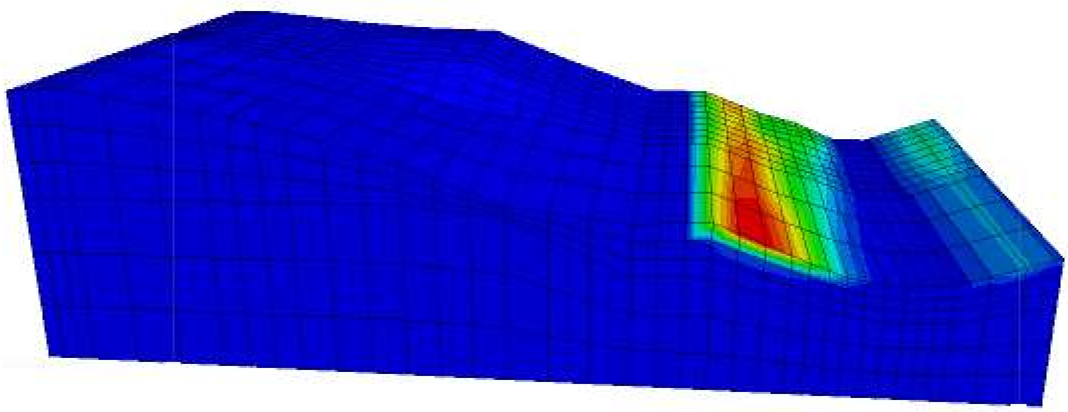

Figure 55 Failure of slope in the Grey-black region

5.3 Orange-brown foundation material in the original design for the tributary diversion

The same values were taken for the Orange-brown material parameters as in table 8. The failure surface looks similar to the failure surface when using the Limit Equilibrium Method. The factor of safety is 1.262.

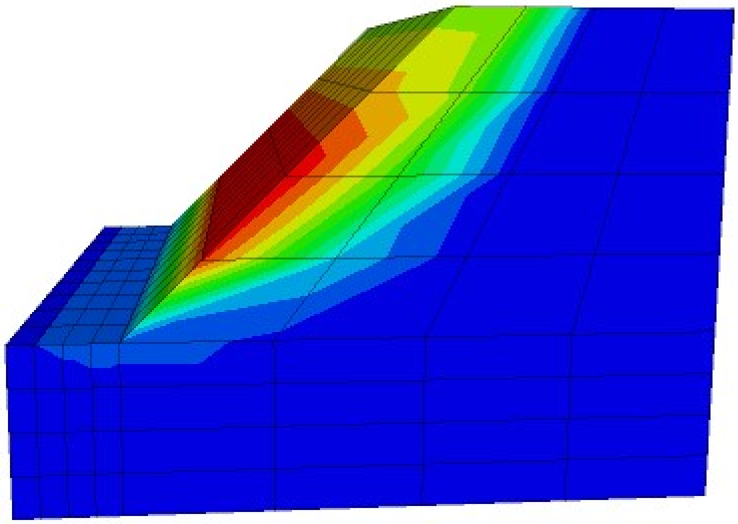

Figure 56 Spring diversion according to the original design 45-degree angle with a FOS of 1.262

6 Comparison of results

The analysis was subdivided into two areas of the dam. The first area is where the interesting geometry exists in the ash segment. In the second area chosen, only the original design for the spring diversion is looked at. The geometry used for the diversion is according to the original design, and the ash is not modelled in. The standard method of extrusion was used in FLAC3D to model the tributary diversion.

Table 10 Comparison of limit equilibrium and numerical results for FOS

	FLAC3D		SLOPE/W	
	Area of Failure	FOS	Area of Failure	FOS
Slope form aerial survey - Orange-brown material	In ash	1.988	In river diversion	1.907
Slope form aerial survey - Grey-black clay	In river diversion	0.846	In river diversion	0.336
45° river diversion in Orange-brown material	From toe to in horizontal	1.262	From toe to in horizontal	0.999

7 Sensitivity analysis

A one-by-one sensitivity analysis was compiled using the two foundation materials prevalent around the dam. As some material parameters are changed, the failure moves from area to area. When the Grey-black material is used, the weakest area occurs in the stream diversion, as shown in figure 50. When the Orange-brown material is analysed, the weakest area starts in the ash, as shown in figure 51, and then as the Orange-brown material is weakened, it moves into the ash zone as shown in figure 50.

A lower limit of 15 and upper of 30 is placed on the Grey-black material's internal angle of friction, and a lower limit of 20 and upper of 40 for the Orange-brown material, based on the typical values given by Das (2011).

When the displacements are looked at, the governing parameters are perceived as Young's Modulus and Poisson's Ratio.

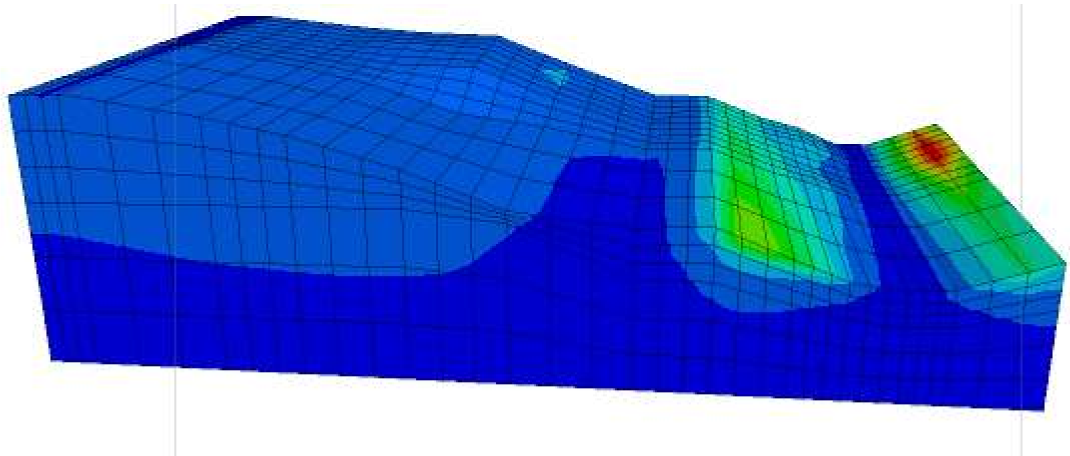

Figure 57 Weakest zone in the spring diversion area, as shown by the displacement plot

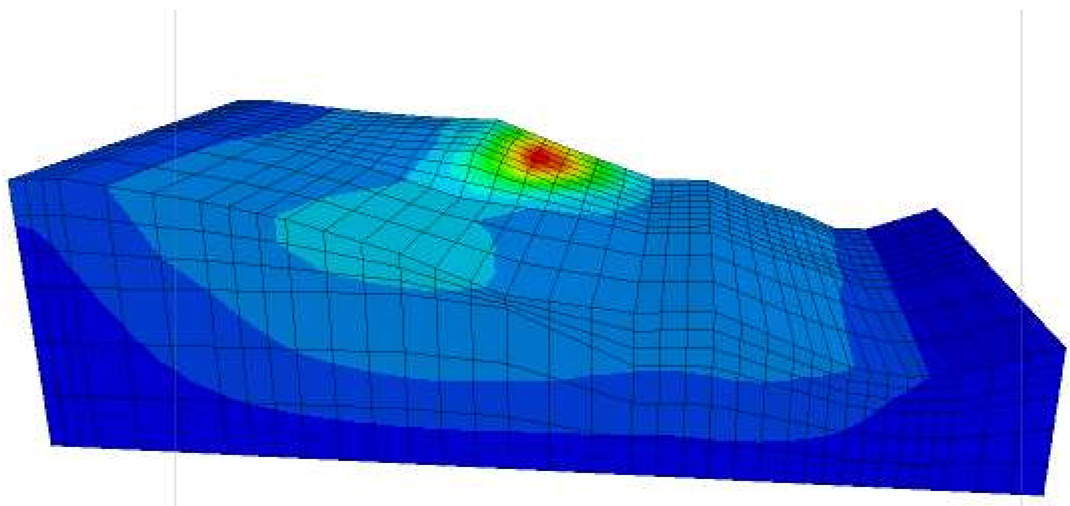

Figure 58 Weakest zone in the ash area, as shown by the displacement plot

7.1 Changing the internal angle of friction and cohesion

7.1.1 Effect of changing the Cohesion and Angle of Friction on the Factor of Safety

7.1.1.1 Changing the cohesion for the Orange-brown material

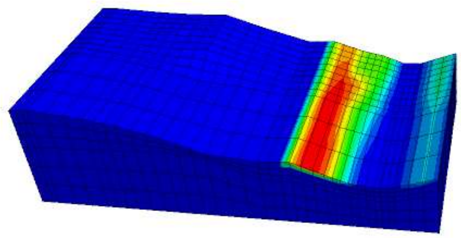

The ash parameters remain unchanged and the Orange-brown material's parameters are changed in 10% intervals.

Table 11 Input parameters for Orange-brown material

Material	Cohesion	Friction	Shear	Young	Density
Fly-ash	0.00E+00	3.85E+01	4.60E-01	5.00E+01	1500
Orange-brown material	5.00E+03	3.00E+01	1.05E+00	1.00E+02	2000

Of note is that the fiction angle changed, which was assigned by FLAC3D. The data is available in Appendix B – table 13.

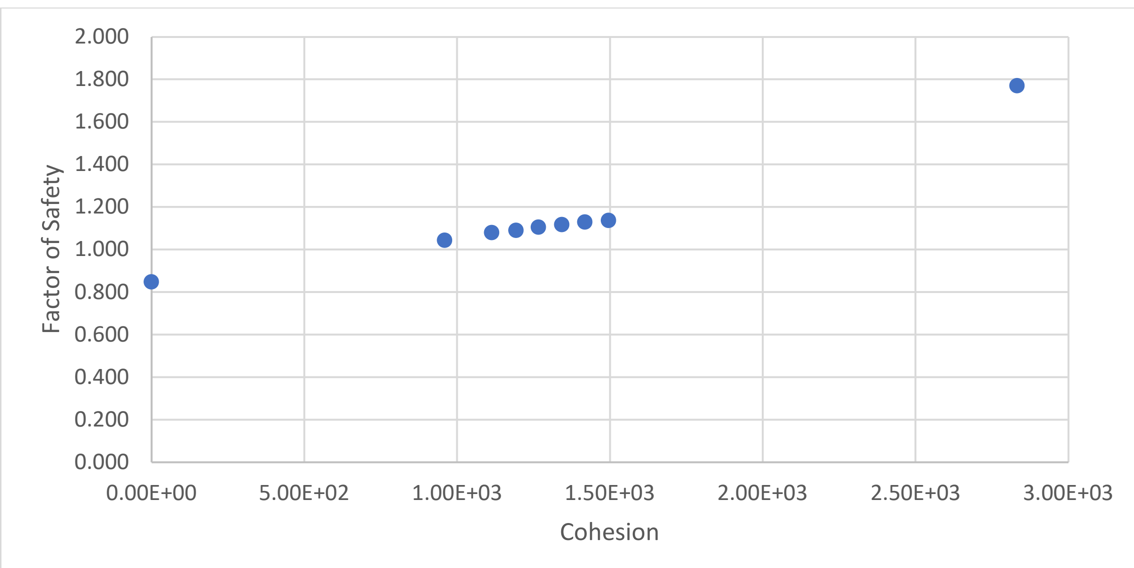

Figure 59 Changing Orange-brown material's cohesion effect on FOS

7.1.1.2 Changing the cohesion for the Grey-black material

Table 12 Input parameters for Grey black material

Material	Cohesion	Friction	Poisson	Young	Density
Fly-ash	0.00E+00	0.00E+00	3.09E-01	5.00E+01	1500
Grey-black material	0.00E+00	1.50E+01	4.30E-01	2.25E+01	2000

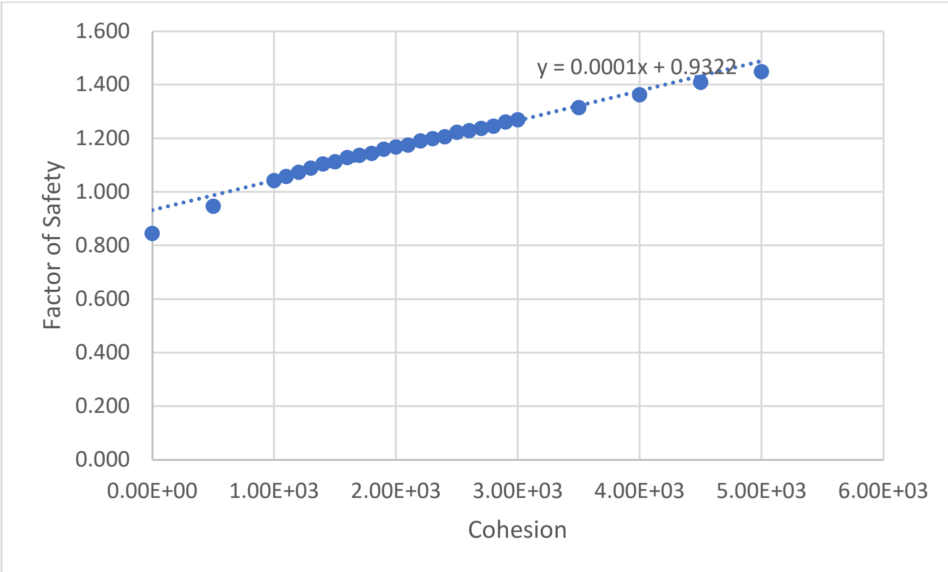

Figure 60 Changing Grey-black material's cohesion effect on FOS

7.1.1.3 Changing the friction angle for the Orange-brown material

The input parameters are:

Material	Cohesion	Poisson	Young	Density
Fly-ash	0.00E+00	3.10E-01	5.00E+01	1500
Orange-brown material	5.00E+03	2.00E-01	1.00E+02	2000

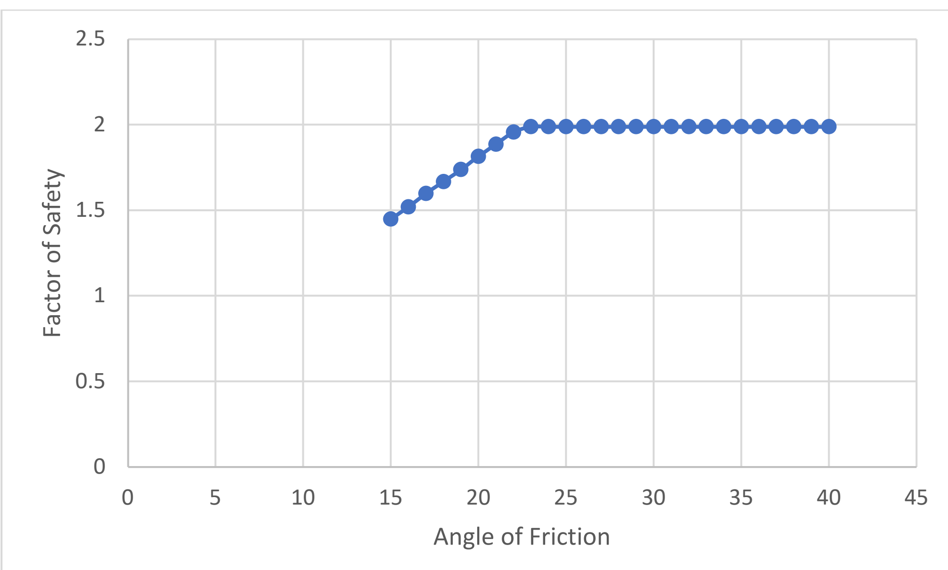

Figure 61 Changing Orange-brown material's friction angle effect on FOS

7.1.1.4 Discussion of results

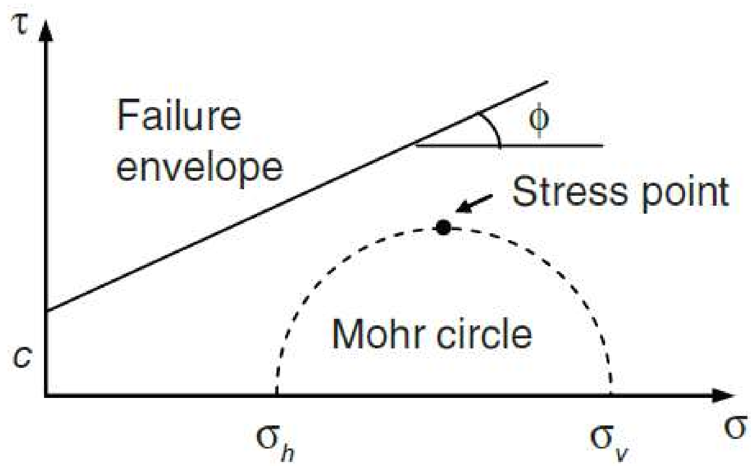

Figure 62 Mohr circle and stress point (Das, 2011)

A linear relationship between the FOS and both cohesion and internal angle of friction, is expected when the Mohr Coulomb method is used. In figure 62, one can see that changing either of these two parameters would linearly affect the FOS.

Of note when looking at figure 62, is the symbol σ for stress. Stress is the force applied over the area it is applied upon, and this is governed by the density of the material and geometry.

For the slopes analysed, the Grey-black material remains unsuitable as a foundation material, even when the cohesion or friction angle was underestimated, as seen in figure 60. Since there is not space between the dam and river diversion to change the geometry of the dam, the areas where this material is present will require retaining walls, major culverts or soil anchors when the trees are removed.

If the internal angle of friction of the Orange-brown material was dramatically overestimated and was below 16°, the dam would not be stable, as seen in figure 61. Above a friction angle of 23° the failure surface moves into the ash region. If the cohesion was overestimated and, was below 2.5kPa, then the dam would once again have a FOS of below 1.5 and be unstable as shown in figure 59.

7.1.2 Displacement when changing Poisson's ratio and Young's modulus

When analysing the effect of changing Poisson's ratio and Young's modulus on displacement, the section in the river is looked at in isolation, please see figure 63. This is done because a failure might occur in the ash material before the foundation material, in this analysis.

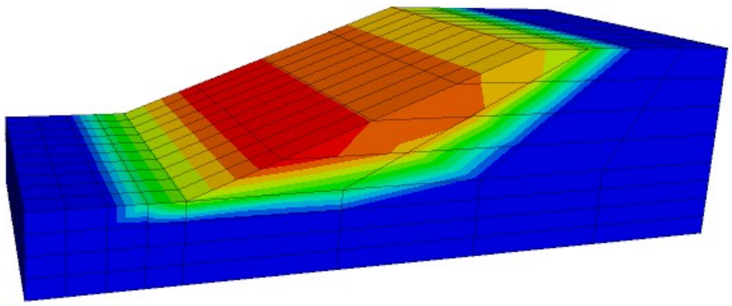

Figure 63 Slip surface in river, when foundation is evaluated in isolation

No initial value for Young's modulus or Poisson's ratio is available for the Orange-brown and a value is arbitrarily chosen, which is in the typical range supplied by (Das, 2011):

Clay	*E* (MPa)
Very soft clay	0.5–5
Soft clay	5–20
Medium clay	20–50
Stiff clay, silty clay	50–100
Sandy clay	25–200
Clay shale	100–200

Figure 64 Typical values for elastic modulus for Grey-blacks (Das, 2011)

Type of Backfill Soil	ν
Loose sand	0.2–0.35
Dense sand	0.3–0.4
Sandy soil	0.15–0.25
Silt	0.3–0.35
Unsaturated clay	0.35–0.4
Saturated clay	0.5
Clay with sand and silt	0.3–0.42

Figure 65 Typical range of Poisson's Ratio (v) (Das, 2011)

As expected, through investigation reflected in the tables in appendix A, the factor of safety remained constant throughout the changes to Poisson's ratio and Young's modulus.

7.1.3 Poisson's Ratio

Poisson's ration relates axial strain to transverse normal strain (Das, 2011). In other words, Poisson's ratio relates the change in length in the axial direction to that in the transverse normal direction under an axial load. The maximum Poisson's ratio is 0.5 for any material. Poisson's ratio, along with Young's modulus can be used to determine the bulk and shear modulus as previously shown. The displacement can be shown in all three directions as shown in figure 66.

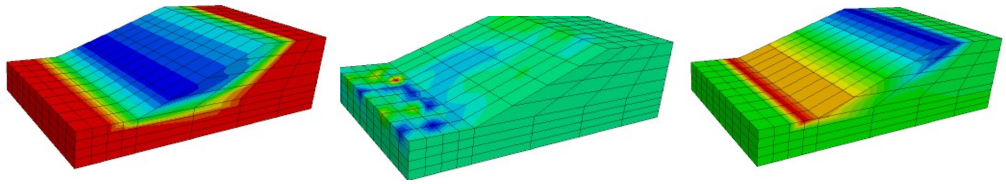

Figure 66 Displacement in x, y and z direction

The Generalised Hooke's Law can be used to express Poisson's ratio in a three dimensional volume as follows (Das, 2011):

$$\tau_x = \frac{1}{E}\left[\sigma_x - v(\sigma_y + \sigma_z)\right]$$

$$\tau_y = \frac{1}{E}\left[\sigma_y - v(\sigma_x + \sigma_z)\right]$$

$$\tau_z = \frac{1}{E}\left[\sigma_z - v(\sigma_x + \sigma_y)\right]$$

$$\sigma_z = \frac{E_1}{(1+v_1)(1-2v_1)}\left[(1-v_1)\frac{\partial w}{\partial z} + (1-v_1)\frac{\partial u}{\partial x}\right]$$

Where

$u = displacement\ in\ x\ direction$
$w = displacement\ in\ z\ direction$
$v = poisson's\ ratio$
$E = Modulus\ of\ elasticity\ or\ Young's\ modulus$
$\tau = strain$
$\sigma = stress$

It can be seen from Hooke's Law that the Poisson's ratio would influence the displacement of the volume because it affects strain. From figure 67 and 68, one can see this effect does not follow a clear pattern. This is because these charts only show the maximum displacement. Poisson's ratio defines how much the strain in one direction relates to the strain in another direction, and hence decreasing or increasing this ratio would cannot be directly related to maximum displacement as seen in figure 67 and 68.

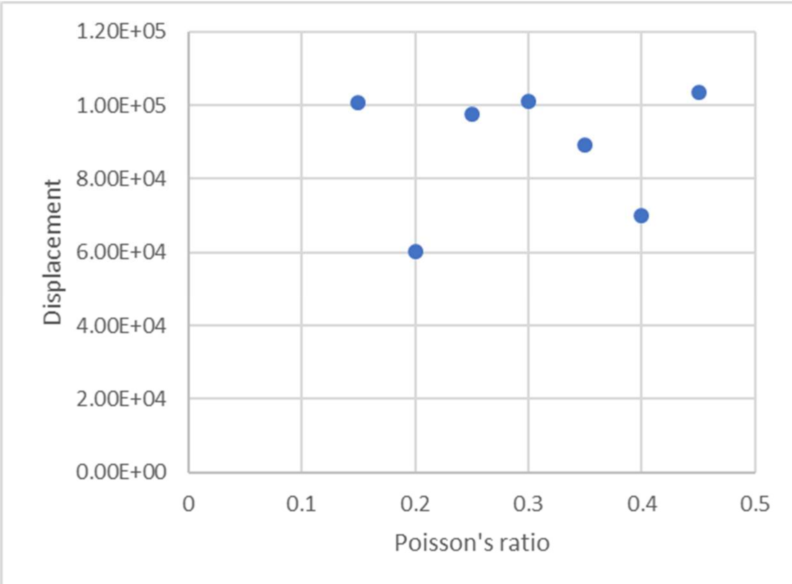

Figure 67 Effect of changing Poisson's ratio on displacement in Orange-brown material

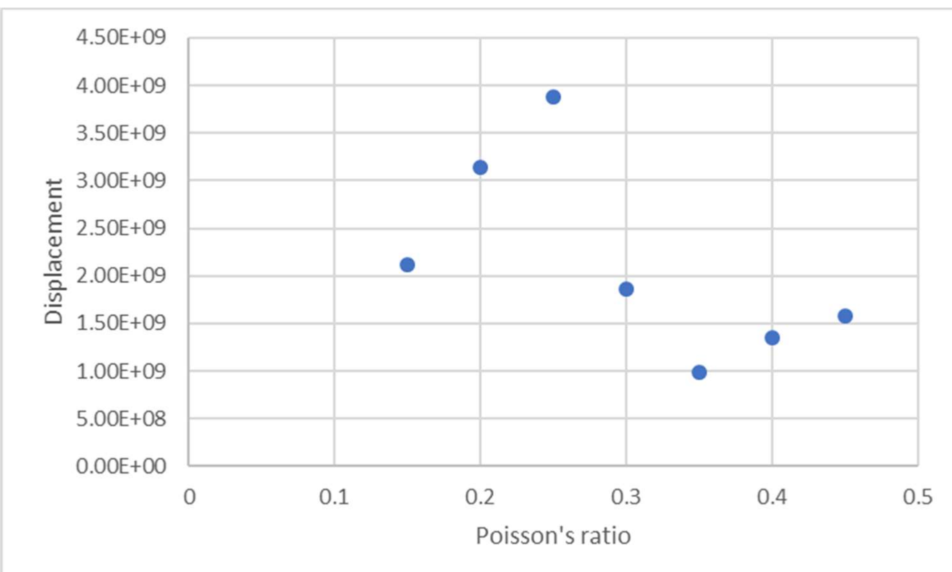

Figure 68 Effect of changing Poisson's ratio on displacement in Grey-black material

7.1.4 Young's Modulus

The Young's modulus or modulus of elasticity show the relationship between stress and strain ($E = \frac{\sigma}{\tau}$). The factor of safety remained at 2.47. Because the FOS remains constant, and the geometry or densities are not changed, changing Young's modulus only changes the strain value. This means that there should be a direct effect on displacement. From figure 67 this effect is seen. Only the maximum displacement is shown in this figure.

Material	Cohesion	Friction	Shear	Young	Density
Fly-ash	0.00E+00	3.40E+01	4.60E-01	5.00E+01	1500
Orange-brown material	5.00E+03	3.00E+01	1.05E+00	Variable	2000

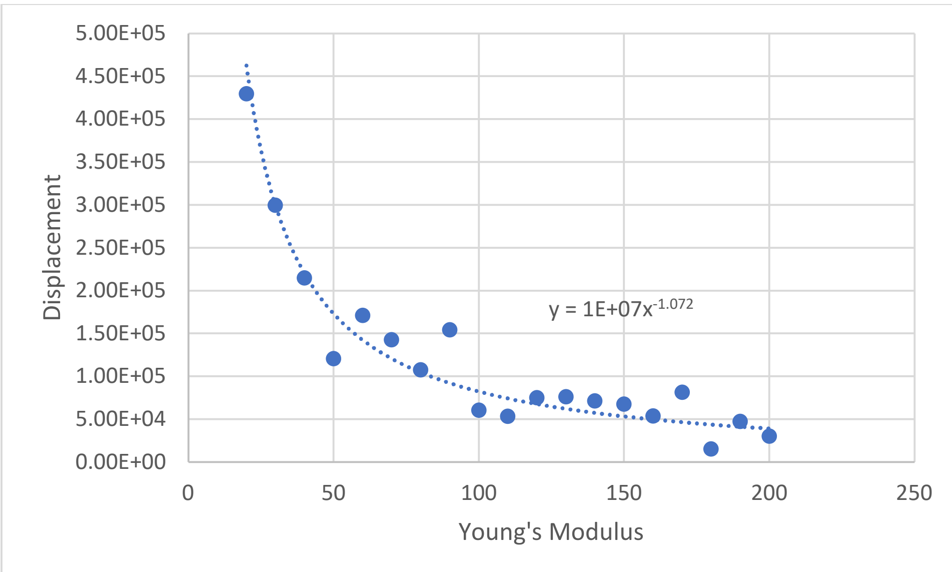

Figure 69 Changing Young's modulus effect on displacement

8 Discussion of results

FLAC3D and Slope/w gave comparable results and as expected, the 3D analysis yielded less conservative values.

The areas in the south of the impoundment, where the river was diverted, has a very weak clay material. This material is not suitable for use in the river diversion as it causes instability.

The areas where the Orange-brown material is present, the slopes appear to be stable. This cannot be true due to the several failures in this material. The cause of these failures could be due to the flow of the river next to the dam, which could cause loss of material and undercutting of the embankment, as shown in figure 71.

When heavy rainfall occurs the stream level rises, removes some of the material and undercuts the trees, trying to correct the slopes of the channel and forming a parabolic profile as shown in figure 70. This creates an unstable slope which fails and causes a ‘land slide’ effect, growing higher into the embankment. Fortunately this is arrested by subsequent tree roots. These roots would act as soil anchors.

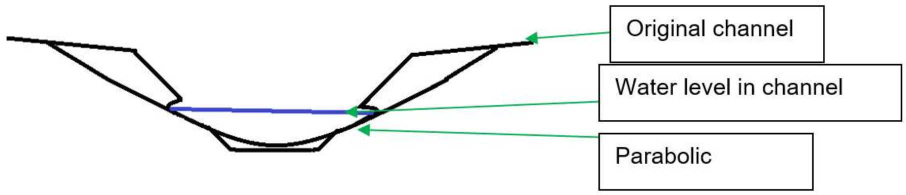

Figure 70 Undercutting of the slopes due to flow

8.1.1 Calculation of bed erosion

Because the internal angle of friction off all the materials are less than the 45° design slope of the channel, the erosion of the side slopes cannot be calculated using Shields Diagram for sedimentation transport. The side slopes should have been designed as below 45°, which is higher than the friction angle of the foundation material.

A density of 2000kg/m³ is used. It is shown that even using a 0.2mm particle size, the bed will be eroded. It is assumed that the smaller particles are washed away, and only Orange-brown material would remain.

$$Slope\ of\ channel\ S_0 = \frac{609.6 + 152.4}{3\ 048\ 000} = 0.00025$$

$$\tau_c = 0.056(\rho_s - \rho)\ \times g \times d = 0.056 \times (2000 - 1000) \times 9.81 \times 0.0002 = 0.11$$

$$\tau_b = \rho \times y \times g \times S_0 = 1000 \times y \times 9.81 \times 0.00025 = 2.45y$$

$$\tau_b \leq \tau_c$$

$$2.45y \leq 0.11$$

$$y \leq 0.073m$$

Slope of the bed (So): 0.00025
Internal angle of friction ϕ: 40°
Density of Orange-brown material ρ_s: 2000kg/m³
Particle size (d): 2mm

y is the maximum depth of flow possible without causing erosion of the bed. This shows that when the particle size is 0.2mm and density is 2000kg/m³ the bed will erode when the flow depth is above 73mm. During storm events this flow occurs.

Figure 71 Erosion damage due to water swirl

9 Conclusion

FLAC3D uses a strength reduction method through a finite volume method in 3 dimensions. This allows for the application of the Mohr-Coulomb failure criteria. This enables the analysis of deformation and the calculation of the factor of safety of slopes.

Using SketchUp Pro and aerial surveys, the modelling in FLAC3D can be made dramatically easier. This modelling is generally considered very time consuming and difficult. SketchUp Pro allows for the creation of skins which can be imported into FLAC3D's building block's tab. A building block can then be created on this skin and draped onto the skin after the building block has been sufficiently discretized.

A good fitting trendline can be drawn onto the graph depicting the effect of changing Young's modulus on displacement. No such relationship is seen between Poisson's ratio and displacement.

Changing the friction angle has a much greater effect on the FOS than changing the cohesion of a soil.

Slope/w uses the limit equilibrium methods in 2-dimensions. It is much easier to use and less time consuming. It allows for several different methods to be used, but for this research the Morgenstern-Price method was used, which is considered the most accurate. 2-Dimensional analyses in general give more conservative results than 3-dimensional analyses. This said, limit equilibrium methods are used most often in practice for slope stability analyses, and these give sufficient results.

10 References

Arpita, B., Sharon, P., Aiswarya Acharath, M., Arash, A., Melanie, S., & Sorakrich, T. (2019). Physical, chemical, and geotechnical properties of coal fly ash: A global review. *Case Studies in Construction Materials, 11*(-). doi:10.1016/j.cscm.2019.e00263

Ayanda, O. S., Fatoki, O. S., Adekola, F. A., & Ximba, B. J. (2012). Characterization of fly ash generated from Matla power station in Mpumalanga, South Africa. *E-Journal of Chemistry, 9*(4), 1788-1795. doi:10.1155/2012/451801

Ayob, A., Zahid, M. Z. A. M., Zaki, M. F. M., Hamid, S. H. A., Yussuf, M. A.-H. M., & Yunus, A. N. M. (2014). Physical, morphological and strength properties of Jana Manjung coal ash mixture for geotechnical applications.(Report). *AENSI Jounrals, 8*(22), 25-29.

Barnard, N. (2010). *Arnot Ash Dam Operations and Maintenance Manual*. ECsoft Pty Ltd. Wierda Park.

Bobet, A. (2010). Numerical Methods in Geomechanics. *The Arabian Journal for Science and Engineering, 35*(1B), 27-48.

Brackley, D., & Erwin, C. (1990). *Arnot Power Station Assessment of the capacity of the existing ash dam complex for Eskom - Megawatt Park*. Retrieved from Johannesburg:

Craig, R. F. (2004). *Criag's Soil Mechanics* (7th ed.). London: Spon Press.

Das, B. M. (2005). *Fundamentals of Geotechnical Engineering* (3rd ed.). United States: Chris Carson.

Das, B. M. (2011). *Geotechnical Engineering Handbook*. Fort Lauderdale, U.S.A.: J.Ross Publishing.

Das, B. M., & Sobhan, K. (2018). *Principles of Geotechnical Engineering* (9th Ed.): Cengage Learning.

Duncan, J. M. (1996). State of the Art: Limit Equilibrium and Finite-Element Analysis of Slopes. *Journal of Geotechnical Engineering, 122*(7), 577-596.

Eskom. (2019). Arnot Power Station. Retrieved from http://www.eskom.co.za/Whatweredoing/ElectricityGeneration/PowerStations/Pages/Arnot_Power_Station.aspx

Fredlund, D. G., & Krahn, J. (1977). Comparison of slope stability methods of analysis. *Canadian Geotechnical Journal, 14*, 429-439.

Google. (2020). Google Maps. Retrieved from https://www.google.com/maps/search/google+maps

Itasca Consulting Group, I. (2017a). FLAC3D6.0 FLAC3D Modeling.

Itasca Consulting Group, I. (2017b). FLAC3D6.0 Theory and Background. In.

Karakuş, D., Özdoğan, M. V., Turan, G., Konak, G., & Onur, A. H. (2018). Investigation of capacity increasing facility of solid waste landfill of thermal power plant: a case study of Yatağan Thermal Power Plant. *Yerbilimleri, 39*(2), 103-116.

Knight, Z. (2015). *Slope Stability analysis of tailings dam embankments.* (Bachelor of Engineering), Charles Darwin University,

Knutsson, R. (2015). *Tailings Dam Performance Modeling and Safety Analysis of a Tailings dam.* Luleå University of Technology, Luleå.

Lebitsa, G. (2016). *Particle Size Segregation and Excess Power Water Pressure with Respect to Rate of Rise of Tailings Dams.* (Philosophiae Doctor (Civil Engineering)), University of Pretoria, Pretoria.

Lekgau, B., Mazibuko, M., & Marais, F. (2019). *Arnot Ash Dam Penstock 8 Design*. Retrieved from Johannesburg:

Li, S., Zhao, J., Chen, Y., & Yang, J. (2005). Optimization research for ash dam cross section. *Advances In Engineering Software, 36*(2), 109-113. doi:10.1016/j.advengsoft.2004.06.008

Lin, Y., Zhou, K., & Li, J. (2018). Prediction of Slope Stability Using Four Supervised Learning Methods. *IEEE Access, 6*, 31169-31179. doi:10.1109/ACCESS.2018.2843787

Ma, Y., Su, P., & Li, Y. (2020). Three-dimensional nonhomogeneous slope failure analysis by the strength reduction method and the local strength reduction method. *Arabian Journal of Geosciences, 21*, 13-14.

Meisheng, F., & Laigui, W. (2011). A tailings dam dynamic stability study based on numerical simulation. In (pp. 1002-1005): IEEE.

Ozcan, N., Ulusay, R., & Isik, N. (2013). A study on geotechnical characterization and stability of downstream slope of a tailings dam to improve its storage capacity (Turkey). *Environmental Earth Sciences, 69*(6), 1871-1890. doi:10.1007/s12665-012-2016-1

Rai, R., Khandelwal, M., & Jaiswal, A. (2011). Application of geogridds in waste dump stability: a numerical modeling approach. *Environmental Earth Sciences, 66*, 1459-1465.

SABS:0286. (1998). Mine residue. In (pp. 1-117). Pretoria: South African Bureau of Standards.

Shen, H., Klapperich, H., Abbas, S. M., & Ibrahim, A. (2012). Slope stability analysis based on the integration of GIS and numerical simulations. *Automation in Construction*(26), 46-53.

Slávik, I. (2013). Stability analysis of the impoundment of ash. *Slovak Journal of Civil Engineers, XXI*(17), 17-23.

Slavik, I., & Skvarka, J. (2019). Intensification of the Ash Impoundment and its Stability Analysis. *IOP Conf. Series: Earth and Environmental Science, 221*.

Verdeș, M. (2017). Stability Analysis of a Coal Combustion Residuals Impoundment. *Mathematical Modelling in Civil Engineering, 13*(2), 27-41. doi:10.1515/mmce-2017-0006

Xu, N., Tian, H., Kulatilake, P. H. S. W., & Duan, Q. (2011). Building a three dimensional sealed geological model to use in numerical stress analysis software: A case study for a dam site. *Computers and Geotechnics, 38*, 1022-1030.

Zhao, X., Xu, J., Youhu, Zhang, C., & Ciao, Z. (2018). Couppled DEM and FDM algorithm for geotechnical analysis. *International Journal of Geomechanics, 18*(6), 1-14.

Zielke-Olivier, J. S. D. R., & Vermeulen, P. D. (2019). A geochemical weathering profile of a fine ash tailings dam and its impact on the underlying aquifers. *Journal of Environmental Management, 242*, 162-170. doi:10.1016/j.jenvman.2019.04.034

Appendix A – Project Specification

ENG4111/4112 Research Project

Project Specification

Student name: Vernon Marc Erasmus

Title: Stability analysis of fossil fuel ash dam at Arnot Power Station

Major: Civil Engineering

Supervisor: Dr. Ali Mirzaghorbanali

Enrolment: ENG4111 – EXT ONL S1, 2020

ENG4112 – EXT ONL S2, 2020

Project Aim: To determine the stability of Arnot Power Station's ash dam using numerical modelling software.

Programme: Version 1, 16 March 2020

1. A comprehensive literature review on the past research study conducted on stability analysis of Geotechnical structures using numerical tools,
2. Review the background data and information on the dam including available geo-technical information and current slopes,
3. Determine the phreatic surfaces in the dam walls,
4. Determine the geo-technical characteristics,
5. Predict the final future geometric shape of the ash dam, and
6. Evaluate the stability of the ash dam using numerical modelling software and limited equilibrium methods.

If time and resources permit:

7. Evaluate the effect of additional drainage installed at the current heights on the overall stability,
8. Evaluate the future life expectation of the dam following current trends in ash supplied to the dam.

Appendix B - Tables

Cohesion's effect on FOS

Table 13 Changing Orange-brown material's cohesion effect on FOS

Number	Material	Bulk	Cohesion	Dilation	Friction	Poisson	Shear	Young	Density
	Fly-ash	1.05E+00	0.00E+00	3.85E+01	3.85E+01	3.09E-01	4.60E-01	1.20E+00	1500
1	Orange-brown material	7.14E+00	0.00E+00	1.75E+01	1.75E+01	4.30E-01	1.05E+00	3.00E+00	2000
	Fly-ash	4.40E-01	0.00E+00	3.29E+01	3.29E+01	3.09E-01	4.60E-01	1.20E+00	1500
2	Orange-brown material	7.14E+00	9.59E+02	1.44E+01	1.44E+01	4.30E-01	1.05E+00	3.00E+00	2000
	Fly-ash	1.05E+00	0.00E+00	3.24E+01	3.24E+01	3.09E-01	4.60E-01	1.20E+00	1500
3	Orange-brown material	7.14E+00	1.04E+03	1.42E+01	1.42E+01	4.30E-01	1.05E+00	3.00E+00	2000
	Fly-ash	1.05E+00	0.00E+00	3.20E+01	3.23E+01	4.30E-01	4.60E-01	1.20E+00	1500
4	Orange-brown material	7.14E+00	1.11E+03	1.40E+01	1.40E+01	3.09E-01	1.05E+00	3.00E+00	2000
	Fly-ash	1.05E+00	0.00E+00	3.18E+01	3.18E+01	3.18E+01	4.60E-01	1.20E+00	1500
5	Orange-brown material	7.14E+00	1.19E+03	1.38E+01	1.38E+01	1.38E+01	1.05E+00	3.00E+00	2000
	Fly-ash	1.00E+00	0.00E+00	2.09E+01	2.09E+01	3.00E+01	4.62E-01	1.20E+00	1500
6	Orange-brown material	5.56E+01	2.83E+03	1.81E+01	1.81E+01	2.00E-01	4.17E+01	1.00E+02	2000
	Fly-ash	1.05E+00	0.00E+00	3.14E+01	3.14E+01	3.09E-01	4.60E-01	1.20E+00	1500
7	Orange-brown material	7.14E+00	1.27E+03	1.36E+01	1.36E+01	4.30E-01	1.05E+00	3.00E+00	2000
	Fly-ash	1.05E+00	0.00E+00	3.11E+01	3.11E+01	3.09E-01	4.60E-01	1.20E+00	1500
8	Orange-brown material	7.14E+00	1.34E+03	1.35E+01	1.35E+01	4.30E-01	1.05E+00	3.00E+00	2000
	Fly-ash	1.05E+00	0.00E+00	3.09E+01	3.09E+01	3.09E-01	4.60E-01	1.20E+00	1500
9	Orange-brown material	7.14E+00	1.42E+03	1.34E+01	1.34E+01	4.30E-01	1.05E+00	3.00E+00	2000
	Fly-ash	1.05E+00	0.00E+00	3.07E+01	3.07E+01	3.09E-01	4.60E-01	1.20E+00	1500
10	Orange-brown material	7.14E+00	1.50E+03	1.33E+01	1.36E+01	4.30E-01	1.05E+00	3.00E+00	2000

	Effective Stress	Factor of Safety	Strain Increment	Strain Rate xx	Stress	Unbalanced force	Velocity	Displacement	Convergence	Local force ratio
Maximum value	0.00E+00	0.848	1.15E+09	1.56E+02	0.00E+00	4.87E+02	7.54E+02	6.29E+09	3.74E+00	3.74E-04
Maximum value	-5.43E+03	1.043	1.15E+09	5.55E+02	-5.43E+03	3.65E+02	5.55E+02	6.31E+09	3.44E-04	5.41E+03
Maximum value	-5.41E+03	1.060	1.15E+09	2.24E+02	-5.41E+03	5.60E+02	1.15E+03	6.30E+09	6.30E+09	5.41E+03
Maximum value	-5.39E+03	1.080	1.15E+09	2.57E+02	-5.39E+03	5.80E+02	1.47E+03	6.31E+09	5.92E+00	5.92E-04
Maximum value	-5.38E+03	1.090	1.15E+09	7.06E+01	-5.38E+03	1.82E+02	4.30E+02	6.30E+09	1.58E+01	1.58E-04
Maximum value	-6.99E+03	1.770	-7.42E+03	2.38E+02	-6.99E+03	2.00E+02	1.34E+03	5.13E+06	5.24E+00	5.13E+06
Maximum value	-5.35E+03	1.105	1.15E+09	6.54E+02	-5.35E+03	1.37E+03	3.97E+03	6.30E+09	2.06E+01	3.00E+00
Maximum value	-5.33E+03	1.117	-9.44E+07	6.01E+02	-5.33E+03	8.98E+02	3.61E+03	6.31E+09	1.12E+01	1.12E-03
Maximum value	-5.32E+03	1.129	1.15E+09	6.69E+02	-5.35E+03	1.29E+03	3.99E+03	6.31E+09	1.28E+01	1.28E-03
Maximum value	-5.31E+03	1.137	-9.42E+07	1.19E+02	-5.31E+03	2.38E+02	7.02E+02	6.31E+09	1.12E+01	2.35E-04

Tables used for Poisson's Ratio

Table 14 Effect of Poisson's Ratio on other parameters in Grey-blackey Orange-brown material and Orange-brown materialy Grey-black

Poisson's ratio	Cohesion	Density	Effective friction angle	Zones	Internal angle of friction	Young	Bulk	Cohesion assigned by FLAC3D	Dilation	Friction assigned by FLAC3D	Shear Modulus
0.15	5000	2000	30	480	30	100	47.619	2.03E+03	1.32E+01	13.163	4.35E+01
0.2	5000	2000	30	480	30	100	55.556	2.03E+03	1.32E+01	13.163	41.667
0.25	5000	2000	30	480	30	100	66.667	2.03E+03	1.32E+01	13.163	40
0.3	5000	2000	30	480	30	100	83.333	2.03E+03	1.32E+01	13.163	38.462
0.35	5000	2000	30	480	30	100	111.11	2.03E+03	1.32E+01	13.163	37.037
0.4	5000	2000	30	480	30	100	166.67	2.03E+03	1.32E+01	13.163	35.714
0.45	5000	2000	30	480	30	100	333.33	2.03E+03	1.32E+01	13.163	34.483

Convergence	Displacement	Effective Stress	FOS	Local Force Ratio	Strain increment	Strain rate	Stress
4.92E+00	1.01E+05	-2.72E+03	2.47E+00	4.92E-04	1.53E+04	2.00E+00	-2.72E+03
1.00E+01	6.04E+04	-2.77E+03	2.47E+00	1.00E-03	9.25E+03	5.09E+00	-2.77E+03
6.42E+00	9.75E+04	-2.71E+03	2.47E+00	6.42E-04	1.48E+04	2.63E+00	-2.71E+03
5.51E+00	1.01E+05	-2.71E+03	2.47E+00	5.51E-04	1.53E+04	2.71E+00	-2.71E+03
5.06E+00	8.91E+04	-2.72E+03	2.47E+00	5.06E-04	1.35E+04	3.43E+00	-2.72E+03
5.39E+00	7.00E+04	-2.75E+03	2.47E+00	5.39E-04	1.06E+04	3.87E+00	-2.75E+03
3.15E+00	1.03E+05	-2.70E+03	2.47E+00	3.15E-04	1.56E+04	2.09E+00	-2.70E+03

Table 15 Effect of Poisson's Ratio on other parameters in Very weak Grey-black

Poisson's ratio	Cohesion	Density	Effective friction angle	Zones	Internal angle of friction	Young	Bulk	Cohesion assigned by FLAC3D	Dilation	Friction assigned by FLAC3D	Shear Modulus
0.15	0	2000	15	480	15	3	1.4286	2.03E+03	1.66E+01	16.641	1.30E+00
0.2	0	2000	15	480	15	3	1.6667	2.03E+03	1.66E+01	16.641	1.25
0.25	0	2000	15	480	15	3	2	2.03E+03	1.66E+01	16.641	1.2
0.3	0	2000	15	480	15	3	2.5	2.03E+03	1.66E+01	16.641	1.1538
0.35	0	2000	15	480	15	3	3.3333	2.03E+03	1.66E+01	16.641	1.1111
0.4	0	2000	15	480	15	3	5	2.03E+03	1.66E+01	16.641	1.0714
0.45	0	2000	15	480	15	3	10	2.03E+03	1.66E+01	16.641	1.0345

Convergence	Displacement	Effective Stress	FOS	Local Force Ratio	Strain increment	Strain rate xx	Stress
3.87E+00	2.12E+09	-4.75E+03	0.90	3.87E-04	3.19E+08	1.24E+02	-4.76E+03
2.71E+00	3.13E+09	-4.89E+03	0.90	2.71E-04	5.08E+08	1.18E+02	-4.89E+03
2.67E+00	3.88E+09	-5.10E+03	0.90	2.67E-04	5.79E+08	9.51E+01	-5.10E+03
2.22E+00	1.86E+09	-5.10E+03	0.90	2.22E-04	3.06E+08	8.69E+01	-5.10E+03
1.37E+00	9.87E+08	-5.10E+03	0.90	1.37E-04	1.67E+08	7.26E+01	-5.10E+03
1.48E+00	1.35E+09	-4.94E+03	0.90	1.48E-04	2.30E+08	5.95E+01	-4.94E+03
1.65E+00	1.58E+09	-4.78E+03	0.90	1.65E-04	2.72E+08	4.87E+01	-2.70E+03

Tables used for Young's Modulus

Table 16 Effect of changing Young's modulus on the Orange-Brown material

Young's Modulus	Cohesion	Density	Effective friction angle	Zones	Internal angle of friction	Poisson's ratio	Bulk	Cohesion assigned by FLAC3D	Dilation	Friction assigned by FLAC3D
20	5000	2000	30	480	30	0.2	11.111	2.03E+03	1.32E+01	13.163
30	5000	2000	30	480	30	0.2	16.667	2.03E+03	1.32E+01	13.163
40	5000	2000	30	480	30	0.2	22.222	2.03E+03	1.32E+01	13.163
50	5000	2000	30	480	30	0.2	27.778	2.03E+03	1.32E+01	13.163
60	5000	2000	30	480	30	0.2	33.333	2.03E+03	1.32E+01	13.163
70	5000	2000	30	480	30	0.2	38.889	2.03E+03	1.32E+01	13.163
80	5000	2000	30	480	30	0.2	44.444	2.03E+03	1.32E+01	13.163
90	5000	2000	30	480	30	0.2	50	2.03E+03	1.32E+01	13.163
100	5000	2000	30	480	30	0.2	55.556	2.03E+03	1.32E+01	13.163
110	5000	2000	30	480	30	0.2	61.111	2.03E+03	1.32E+01	13.163
120	5000	2000	30	480	30	0.2	66.667	2.03E+03	1.32E+01	13.163
130	5000	2000	30	480	30	0.2	72.222	2.03E+03	1.32E+01	13.163
140	5000	2000	30	480	30	0.2	77.778	2.03E+03	1.32E+01	13.163
150	5000	2000	30	480	30	0.2	83.333	2.03E+03	1.32E+01	13.163
160	5000	2000	30	480	30	0.2	88.889	2.03E+03	1.32E+01	13.163
170	5000	2000	30	480	30	0.2	94.444	2.03E+03	1.32E+01	13.163
180	5000	2000	30	480	30	0.2	100	2.03E+03	1.32E+01	13.163
190	5000	2000	30	480	30	0.2	105.56	2.03E+03	1.32E+01	13.163
200	5000	2000	30	480	30	0.2	111.11	2.03E+03	1.32E+01	13.163

Shear	Convergence	Displacement	Effective Stress	FOS	Local Force Ratio	Strain increment	Strain rate	Stress
8.3333	6.6472	4.30E+05	-2.72E+03	2.47	6.65E-04	6.54E+04	1.70E+01	1.70E+01
12.5	6.9119	3.00E+05	-2.72E+03	2.47	6.91E-04	4.56E+04	9.99E+00	9.99E+00
16.667	6.6472	2.15E+05	-2.72E+03	2.47	6.65E-04	3.27E+04	8.51E+00	8.51E+00
20.833	10.02	1.21E+05	-2.77E+03	2.47	1.00E-03	1.85E+04	1.02E+01	1.02E+01
25	3.6829	1.71E+05	-2.72E+03	2.47	3.68E-04	2.59E+04	3.38E+00	3.38E+00
29.167	4.8272	1.43E+05	-2.72E+03	2.47	4.83E-04	2.17E+04	3.15E+00	3.15E+00
33.333	6.6472	1.07E+05	-2.72E+03	2.47	6.65E-04	1.63E+04	4.26E+00	4.26E+00
37.5	2.8327	1.54E+05	-2.69E+03	2.47	2.83E-04	2.31E+04	1.53E+00	1.53E+00
41.667	10.02	6.04E+04	-2.77E+03	2.47	1.00E-03	9.25E+03	5.09E+00	5.09E+00
45.833	9.8414	5.33E+04	-2.78E+03	2.47	9.84E-04	8.14E+03	4.69E+00	4.69E+00
50	6.9119	7.49E+04	-2.72E+03	2.47	6.91E-04	1.14E+04	2.50E+00	2.50E+00
54.167	3.95	7.61E+04	-2.72E+03	2.47	3.95E-04	1.55E+04	1.86E+00	1.86E+00
58.333	4.8272	7.14E+04	-2.72E+03	2.47	4.83E-04	1.08E+04	1.57E+00	1.57E+00
62.5	3.5626	6.75E+04	-2.72E+03	2.47	3.56E-04	1.02E+04	1.47E+00	1.47E+00
66.667	6.6472	5.37E+04	-2.72E+03	2.47	6.65E-04	8.17E+03	2.13E+00	2.13E+00
70.833	2.726	8.14E+04	-2.69E+03	2.47	2.73E-04	1.22E+04	8.22E-01	8.22E-01
75	14.541	1.51E+04	-3.00E+03	2.47	1.45E-03	2.30E+03	3.75E-01	3.75E-01
79.167	5.9435	4.76E+04	-2.72E+03	2.47	5.94E-04	7.23E+03	1.62E+00	1.62E+00
83.333	10.02	3.02E+04	-2.77E+03	2.47	1.00E-03	4.63E+03	2.54E+00	2.54E+00